Title
Performance Analysis of XCPC Powered Solar Cooling Demonstration Project

Author
Widyolar, Bennett

Publication Date
2013

Peer reviewed|Thesis/dissertation

UNIVERSITY OF CALIFORNIA, MERCED

Performance Analysis of XCPC Powered Solar Cooling Demonstration Project

A Thesis submitted in partial satisfaction of the requirements

for the degree of Master of Science

in

Mechanical Engineering and Applied Mechanics

by

Bennett K. Widyolar

Committee in charge:

Professor Gerardo Diaz, Chair

Professor Roland Winston

Professor Yanbao Ma

Spring 2013

The Thesis of Bennett Kuang Tai Widyolar is approved, and it is acceptable in quality and form for publication on microfilm and electronically:

Roland Winston

Yanbao Ma

Gerardo Diaz, Program Chair

University of California, Merced

2013

Table of Contents

List of Symbols

A_{col} solar collector inlet aperture area (m^2)

C_p specific heat capacity (J/kg-K)

COP coefficient of performance

$I_{\odot}$ solar irradiance (W/m^2)

$\dot{m}$ mass flow rate (kg/s)

Q thermal power (W)

T temperature (° C)

W work (W)

Greek letters

η efficiency

Δ delta

Subscripts

chl chilled water

col collectors

Abbreviations

CFM - Cubic Feet per Minute

COP - Coefficient of Performance

DNI - Direct Normal Irradiance

EG - Ethylene Glycol

EVT - Evacuated Tube Collector

EW - East / West

FPC - Flat Plate Collector

GPM - Gallons per Minute

GTI - Global Tilted Irradiance

HP - Horsepower

HVAC - Heating, Ventilation, and Air Conditioning

kW - Kilowatt

kWh - Kilowatt Hour

LiBr - Lithium Bromide

NS - North / South

PSP - Precision Spectral Pyranometer

TMY - Typical Meteorological Year

UC - University of California

XCPC - External Compound Parabolic Concentrator

List of Figures

List of Tables

1. Introduction

Modern solar thermal technologies have been successfully demonstrated since the 1970s. Solar thermal collectors are generally classified into two basic regimes: low temperature and high temperature. Low temperature collectors are usually simple non concentrating systems (flat plates, evacuated tubes) that work best below 100 °C and are used primarily for water heating. High temperature collectors (parabolic trough, linear Fresnel, power tower) generally require a tracking mechanism to concentrate a large number of suns onto a small receiver and are designed to operate above 300 °C. The temperature range 100 – 300 °C is not well served by current solar collectors, even though there exists a huge potential market since a large number of processes require heat in this temperature range.

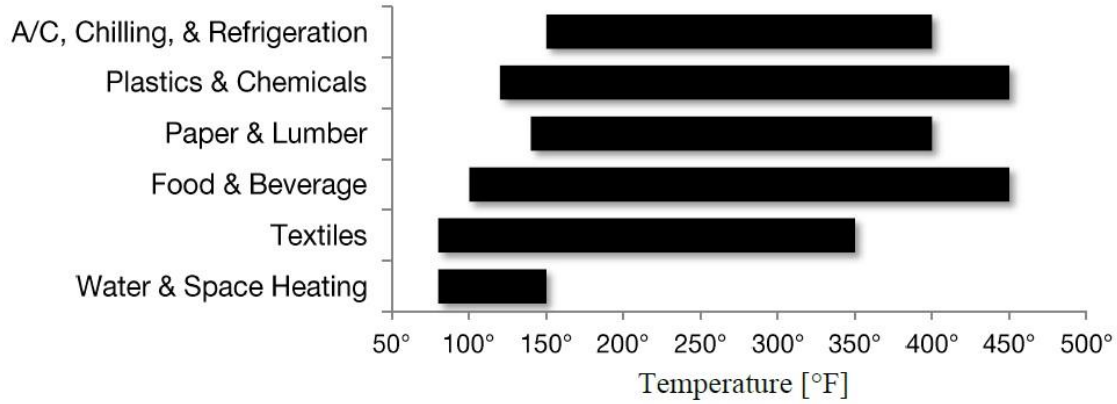

Figure 1 – Process Heat Applications

The primary reason for this is that low temperature collectors do not have the efficiency to operate at higher temperatures and high temperature collectors are only economic on very large scales and are often too costly for medium temperature range applications.

This thesis is part of the ongoing work of UC Solar at the UC Merced campus in developing solar thermal collectors that can efficiently deliver thermal power in the temperature range 100 – 300 °C. It is based on the foundational work done by Kevin Balkoski in testing and quantifying the performance of several different XCPC designs, and Heather Poiry who led the design and construction of the XCPC powered solar cooling system discussed here. This thesis will summarize their previous works and present performance data for the solar cooling system, as well as a discussion on maintenance, current obstacles, and improvements for future systems.

1.1 Motivation for Solar Cooling

Current energy systems based on fossil fuels are largely responsible for the present humanitarian, environmental, and economic crisis. World energy demand – and corresponding $C0_2$ emissions – is expected to rise with the rapid development of many countries around the world. The continued rise in both living and working comfort conditions and reduced prices for conventional (electrical) air conditioning units has led to a fast proliferation of these systems. In residential buildings, these are low efficiency systems associated with significant contributions to peak electricity demand. At the same time there remains the looming question as to how much usable fossil fuel actually remains available. These trends are the catalyst calling for new models in heat and power generation and encouraging strategies that include renewable energies with higher levels of efficiency to reduce dependence on fossil fuels and the emissions they produce and to offset peak power consumption. In

this framework, solar and hybrid technologies represent a potential solution in the near future.

Solar cooling has long been a desired goal in utilizing the solar resource for the benefit of people. The reasons are intuitive; the resource is well-matched to the load (high cooling demand days are usually sunny days) and if deployed on a roof, solar radiation that would otherwise heat the building is instead diverted to cool the building. There is also an enormous potential to reduce energy consumption and harmful emissions as buildings account for about 41% of primary energy consumption in the United States (most of which is used for space heating and cooling, water heating, refrigeration, and lighting [1]) and are associated with about 40% of the United States' carbon dioxide emissions [2]. Solar cooling also leads to a reduction of peak electricity demand, which is a benefit for the electricity network and could lead to cost savings of the most expensive peak electricity. However; the technical barriers to implementation are well-known. Efficient cooling machines require relatively high temperatures which are often beyond the range of flat plate solar collectors, while tracking collectors are problematic for building applications.

1.2 History of Solar Cooling

During the 1970s and 1980s there was a significant amount of work done in the USA and Japan on the development of solar cooling components and systems and a number of demonstration projects proved technical feasibility. These systems, however, failed to establish a significant global market for solar thermal cooling due to their high initial cost, lack of commercial hot water driven chillers, and a scarcity of demonstrations and impartial assessments by reputable institutions [3]. Recently,

there has been a renewed interest in the field of solar cooling with the development of high temperature solar receivers and the commercial availability of hot water driven chillers. Research and demonstration projects have been carried out in many countries, particularly in the US, Germany, and Spain, and under the framework of the Solar Heating and Cooling Programme of the International Energy Agency (IEA). Yet despite the existence of long term demonstration projects and even after ten years of numerous activities in the field of solar cooling, market penetration remains small [4]. Currently there exists a good supply of robust, cost effective solar collectors produced on an industrial level that operate with temperatures below 110 °C, but solar collectors for higher temperatures above approximately 130 °C are still scare as they are a relatively young technology and not yet broadly applied. However, there exists a potential for important cost savings that may be achieved by developing advanced materials and production technologies [4]. Major progress in the last decade was made towards the development of small capacity thermally driven chillers (down to 5 kW) and there are several R&D projects focused on continuing to develop the technology of absorption chillers[5, 6, 7], adsorption chillers [8], and open cooling cycles using liquid desiccants [9, 10]. These developments have the potential to increase efficiencies, make such systems more compact, lower required operating temperatures, and lower system costs. Completely different solutions, such as new thermo-mechanical cycles, promise a significant increase in efficiency and are under development but have not yet left laboratory scale. Ultimately, continued development of both cooling machines and high temperature solar collectors is needed to reach technical maturity and realize

on potential cost savings that will make solar cooling systems economically competitive.

1.3 Technical Quantification

A basic parameter of any cooling system is the coefficient of performance (COP), which is defined as the useful cold (Q_{cold}) produced per unit driving heat (Q_{heat}) and gives a measure of the system's ability to produce cooling from heat.

$$COP = \frac{Q_{cold}}{Q_{heat}} \quad (1)$$

There are several technologies that can produce cooling from a driving heat source (sorption chillers, dessicant systems, thermomechanical systems), but absorption chillers are the dominant technology for solar cooling primarily because the technology is well developed and they are commercially available in a wide range of capacities [11].

Absorption chillers use a refrigerant-sorption chemical pair to transfer heat through a series of chambers of high and low pressure. The most common chemical pair for air conditioning applications is water-LiBr. The simplest of these machines are called single effect LiBr chillers and operate with a COP of about 0.7 using a heat source between 80 - 100 °C. These chillers are well matched for stationary solar collectors, such as flate plate collectors or evacuated tube collectors, which can easily achieve this temperature range. Double effect Li-Br chillers require operating temperatures between 140-160 °C but can produce nearly twice as much cooling (COP $\approx$ 1.1-1.2) as their single effect counterparts for the same energy input. Thus a double effect system can theoretically produce the same amount of cooling as a

single effect system with half the collector field area if they can utilize the benefits of higher temperature heat that can be provided by certain types of solar collectors. Triple effect chillers, which can potentially reach a COP of 1.7 with driving temperatures above 160 °C, are an exciting possibility for future projects but are still under development [12].

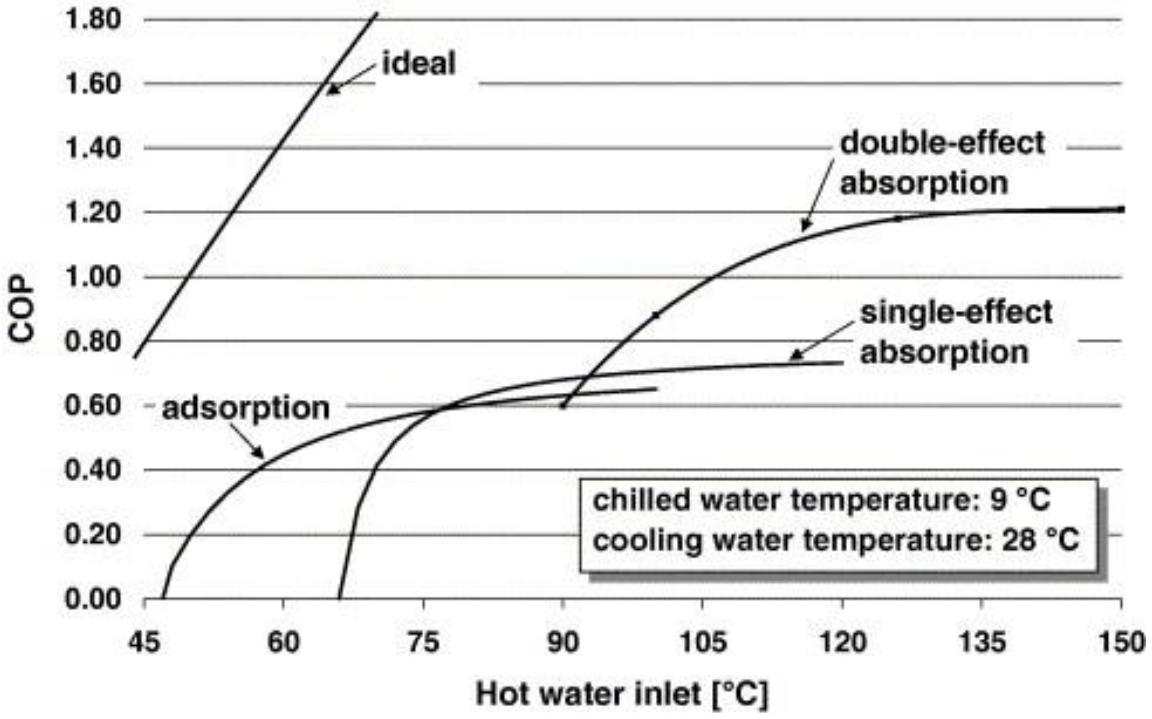

Figure 2 - COP curves

The performance of a solar cooling system can be characterized by three basic parameters: collector efficiency (η_{col}), thermal coefficient of performance ($COP_{thermal}$), and the solar COP (COP_{solar}). Collector efficiency is the fraction of available solar power incident on the collector (Q_{solar}) that is converted into usable heat power (Q_{col}) by the collectors.

$$\eta_{col} = \frac{Q_{col}}{Q_{solar}} = \frac{\dot{m} C_p \Delta T_{col}}{I_{\odot} A_{col}} \quad (2)$$

For high concentration tracking collectors it is customary to consider only beam radiation (DNI) as the available solar energy incident on the collector ($I_{\odot}$) because this is the only radiation they can collect. For non-concentrating collectors, total hemispherical radiation on the plane of the collector field is the relevant quantity. Concentrating stationary collectors (such as the XCPC) are a mix of both worlds because they can accept direct light as well as a certain fraction of diffuse light. For these collectors, C_x corrected radiation (C_x = DNI + Diffuse/C) is the proposed quantity for the amount of available solar radiation incident on the collector.

We define the thermal COP of a solar cooling system to be the ratio of cooling output per unit usable heat captured by the solar collectors. This term includes the COP of the chiller as well as thermal losses through insulation, storage tanks, heat exchangers, and any other component between the collectors and the chiller.

$$COP_{thermal} = \frac{Q_{cold}}{Q_{col}} = \frac{\dot{m}C_p\Delta T_{chl}}{\dot{m}C_p\Delta T_{col}} \tag{3}$$

The solar COP is the ratio of cooling output per available solar power and characterizes the overall performance of the system, including the collectors and all thermal losses throughout the system.

$$COP_{solar} = \frac{Q_{cold}}{Q_{solar}} = \frac{\dot{m}C_p\Delta T_{chl}}{I_{\odot}A_{col}} \tag{4}$$

Parasitic losses from electrical pumping power and chiller power can also be included to give a parasitic solar COP.

$$COP_{solar,parasitic} = \frac{Q_{cold}}{Q_{solar} + W_{electrical}} \tag{5}$$

When calculated for a single moment in time, these are considered instantaneous quantities and can have significant variation over the course of operation due to the high variability of solar radiation and the latency between components in a solar cooling system. To rectify this, an average or daily value is often presented.

1.4 Current Systems

Several solar assisted cooling projects have been demonstrated in the past 15 years and they are presented here to gain a basic understanding of the performance of solar cooling systems to date. A flat plate collector (FPC) system in Madrid, which drove a single effect water/LiBr absorption chiller, achieved an overall solar COP of about 0.11 [13]. This system is admittedly a poorly performing system and should in fact operate in the range of 0.2-0.3. An evacuated tube (EVT) collector system in Wales powered a small LiBr/H20 absorption chiller with an overall solar COP of about 0.4 [14]. A combined FPC and EVT system powered a single effect LiBr/H20 absorption chiller in New Mexico with an overall solar COP of about 0.25 [15].

Figure 3 – Flat Plate Collector

Figure 4 – Evacuated Tube Collector

Several high temperature solar cooling systems powering double effect chillers have also been demonstrated. A linear Fresnel collector system in Seville drove a double effect LiBr/H20 absorption chiller with a solar COP of approximately 0.44 [16], and a parabolic

Figure 5 – Linear Fresnel Solar Plant

trough system in Pennsylvania drove a double effect LiBr/H20 absorption chiller with a solar COP of approximately 0.35 [17]. Also in 1998 a double effect LiBr/H20 absorption chiller was run by a field of non-tracking integrated compound parabolic concentrators (ICPC) in California and achieved a solar COP of almost 0.5 [18]. These were non-concentrating evacuated tubes that performed exceedingly well, but failed to be even remotely economical. Linear Fresnel and parabolic trough collector systems require single axis tracking mechanisms to concentrate by large factors and thus can achieve temperatures much higher than those needed by a double effect absorption chiller.

Figure 6 – Parabolic Trough Collector

In 2009, researchers from the UC Solar group at University of California, Merced built a solar cooling system to assess the feasibility of a new type of non-tracking solar collector, the external compound parabolic concentrator (XCPC), in providing power for a double effect LiBr + H_20 absorption chiller. This is the first system to combine the XCPC, a medium temperature (up to 200 °C) non tracking collector, with a double effect chiller. The main benefit of this collector lies in its ability to reach the operating

temperatures required by a double effect LiBr absorption chiller without the need for tracking. The XCPC collectors and cooling system were designed, constructed, and tested for two cooling seasons, and the performance results are presented in this thesis.

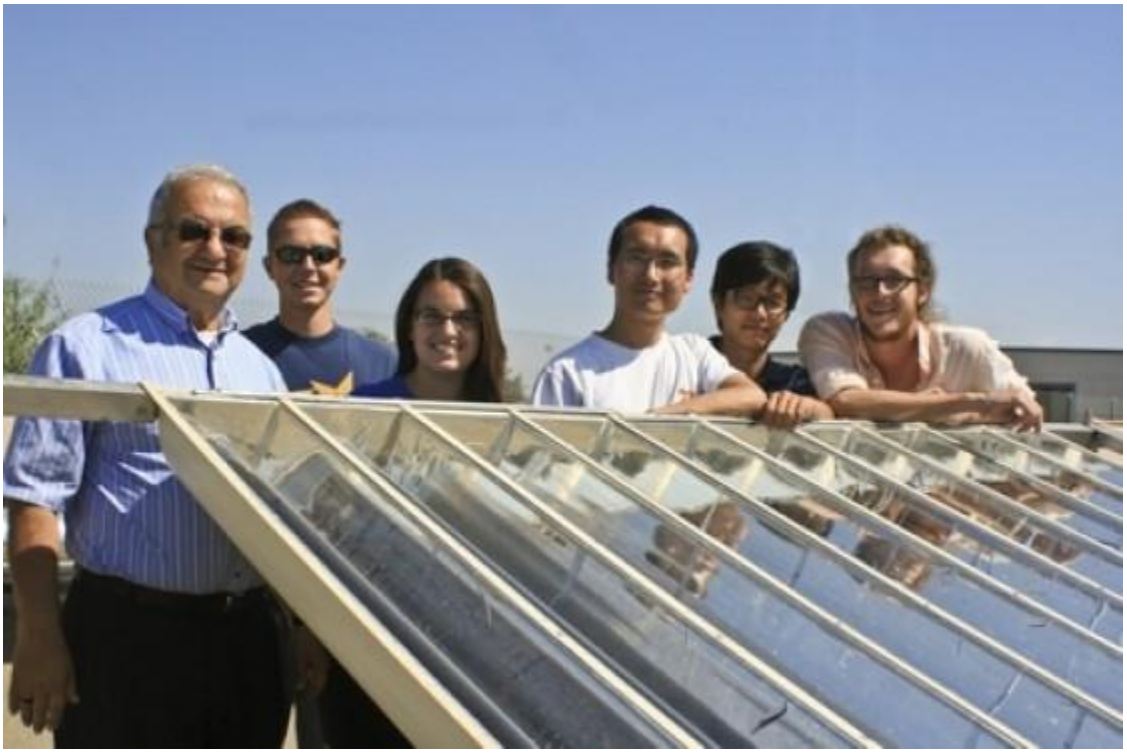

Figure 7 – XCPC Collector, Roland Winston, and Solar Cooling Team

2. System Description

This solar cooling system was designed, constructed, and tested by the UC Solar group at the UC Merced Castle Research facility. The system is powered by 160 XCPC type trough collectors (53.3 m^2 total inlet aperture), installed facing true south at a 20 degree inclination to provide maximum power during the Merced (37 °N) summer. They collect and convert solar energy by heating a mineral oil (Duratherm 600) which is circulated by a pump. Heat is transferred to an aqueous solution containing 40% ethylene glycol by a heat exchanger (90% efficiency at operating conditions) which is then circulated into a 23 kW LiBr-water double effect absorption chiller (see Fig. 8).

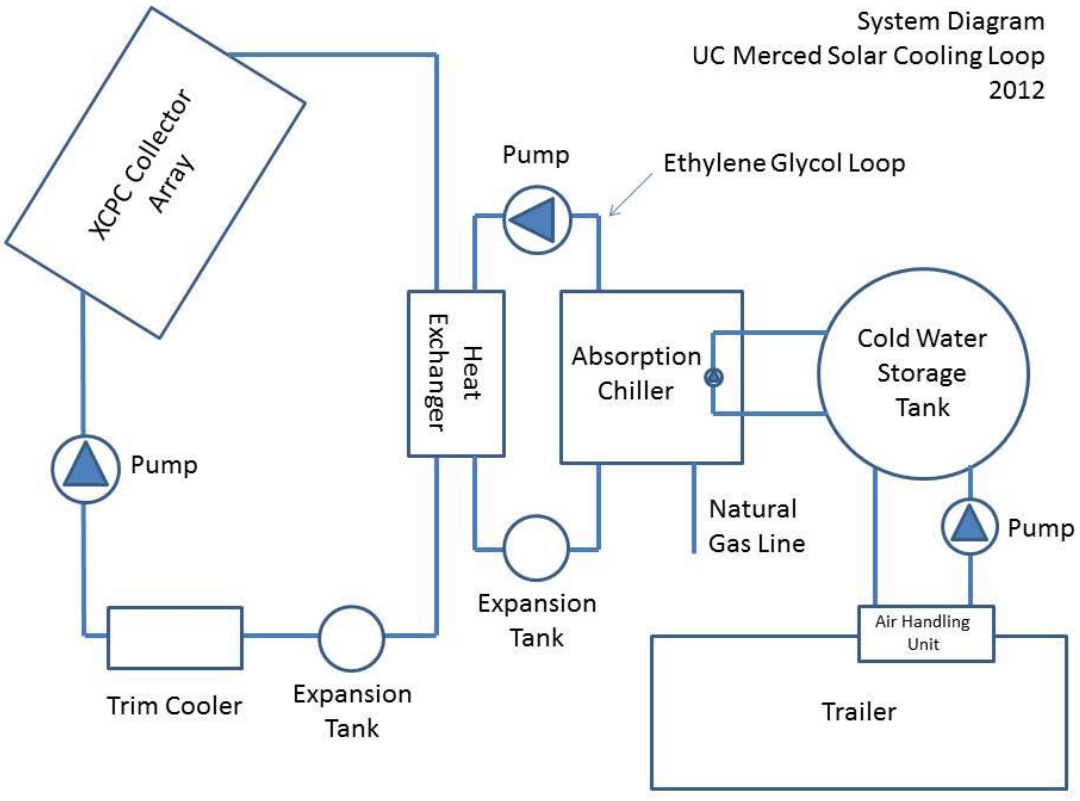

Figure 8 – System Diagram

The intermediate ethylene glycol loop was installed because the chiller manufacturer (BROAD) would not guarantee their warranty if a paraffin-based fluid (mineral oil) was pumped through their chiller. However, they have since retracted their issue with paraffin-based substances and in the future an intermediate loop will not be necessary (in fact we are currently in the process of removing this loop for summer 2013). Water is cooled by the chiller and pumped into a 500 gallon storage tank. This water is circulated by an auxiliary pump from the tank into an air handling unit that provides cooling for a small 720 sq. foot trailer. A trim cooler was installed on the collector loop to release heat form the system in case of emergencies or overheating.

All hot pipes were insulated using 2" thick fiberglass pipe insulation (0.056 W/m-K). The manifolds were insulated using Microtherm (0.022 W/m-K), a high temperature insulation, and then covered with FiberFrax (0.046 W/m-K), a high temperature fiberglass blanket. Heat loss from all hot pipes and manifolds was estimated to be 1.4 kW and 1.5 kW respectively.

$$Q_{net} = Q_{col} - Q_{loss} = I_{\odot} A_{col} \eta_{col} - (Q_{pipes} + Q_{manifolds}) \quad (6)$$

Thus assuming 1000 W/m^2 of incoming radiation and a collector efficiency of about 0.45, the collectors will provide a little over 21 kW of net thermal power to the chiller. More specific information on the selection and sizing of components and overall design of the system can be found in Heather Poiry's thesis, "Efficient Solar Cooling" [22].

2.1 The External Compound Parabolic Concentrator (XCPC)

The collector configuration is an evacuated tube receiver matched to an external non-imaging reflector, typically referred to as an XCPC. Figure 10 is an image of the prototype. The XCPC provides solar concentration without moving parts and can achieve operating temperatures up to 200°C. The design principle maximizes the probability that radiation starting at the receiver would be directed to a specific band in the sky we wish to accept. In our case (north-south orientation) this band is 120 degrees in azimuth and 180 degrees in elevation. This corresponds to a nominal operational time period of eight hours per day with a concentration ratio of 1.18 [19].

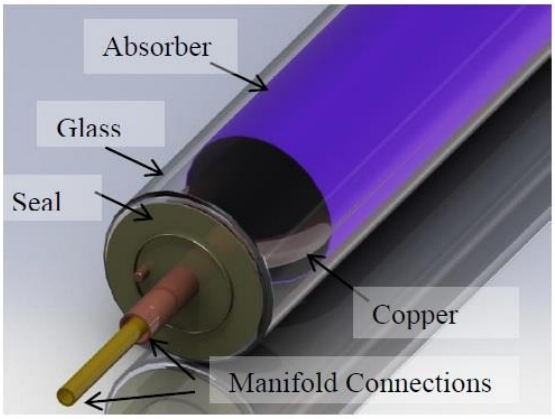

Figure 9 – Vacuum Tube

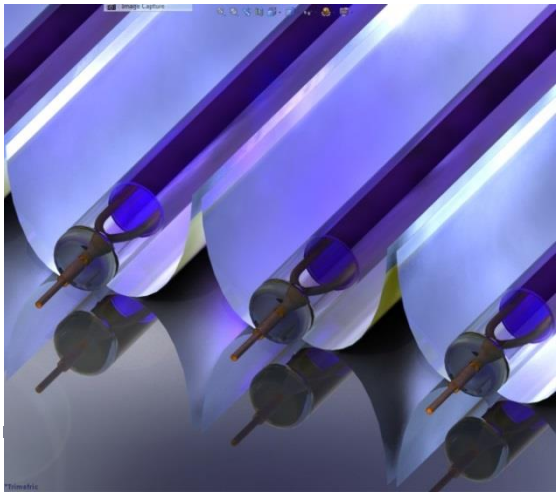

Figure 10 – XCPC design rendering

Inside the evacuated tube receiver is a metallic absorber with a selective coating designed to absorb as much of the solar spectrum as possible while minimizing emission at operating temperatures. Heat is transferred from the metallic absorber to a tube on the inside via conduction, which transfers heat to the fluid passing through it. The space between the absorber and the glass shell is evacuated so that convection and conduction are eliminated and heat is lost from the

hot absorber to the external glass shell only by radiation. As a result, these collectors are efficient even at high operating temperatures.

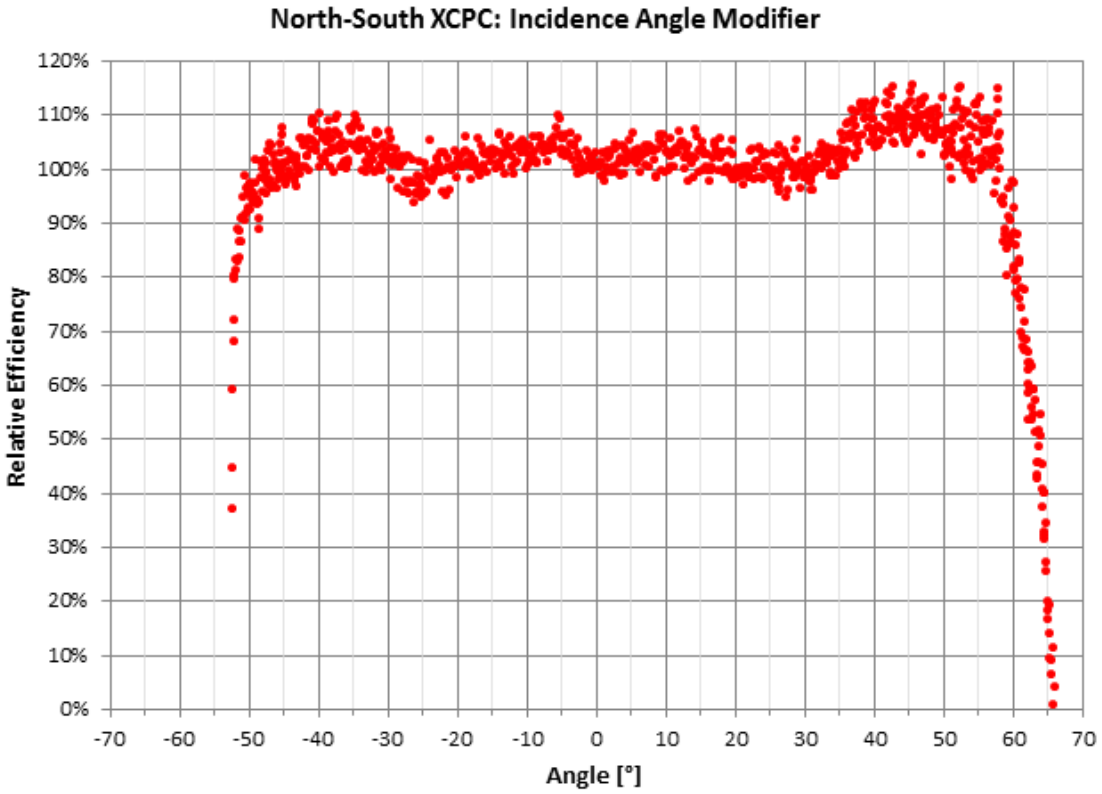

Figure 11 – XCPC Angular Acceptance

The XCPCs used in this solar cooling system were designed to operate facing North-South and to accept light within a 60 degree half angle. The efficiency of the XCPC over a range of acceptance angles is presented in Figure 5. This design was chosen so that the XCPCs would "see" the sun, which moves at approximately 15 degrees azimuthally every hour, for about 8 hours. The selective coating on the absorber had a solar weighted absorptance of 0.902 and an emittance that ranged from 0.05 to 0.14 at 25 and 200 °C respectively. The troughs were produced locally from ABS plastic sheet and lined with ReflecTech, a silver film with spectral and hemispherical reflectance exceeding 94% [20]. A high optical efficiency (71.3%)

coupled with the ease of non-tracking make the XCPC collector an ideal collector for medium range temperature applications (up to 200 °C), the demonstration of which was the motivation for this project.

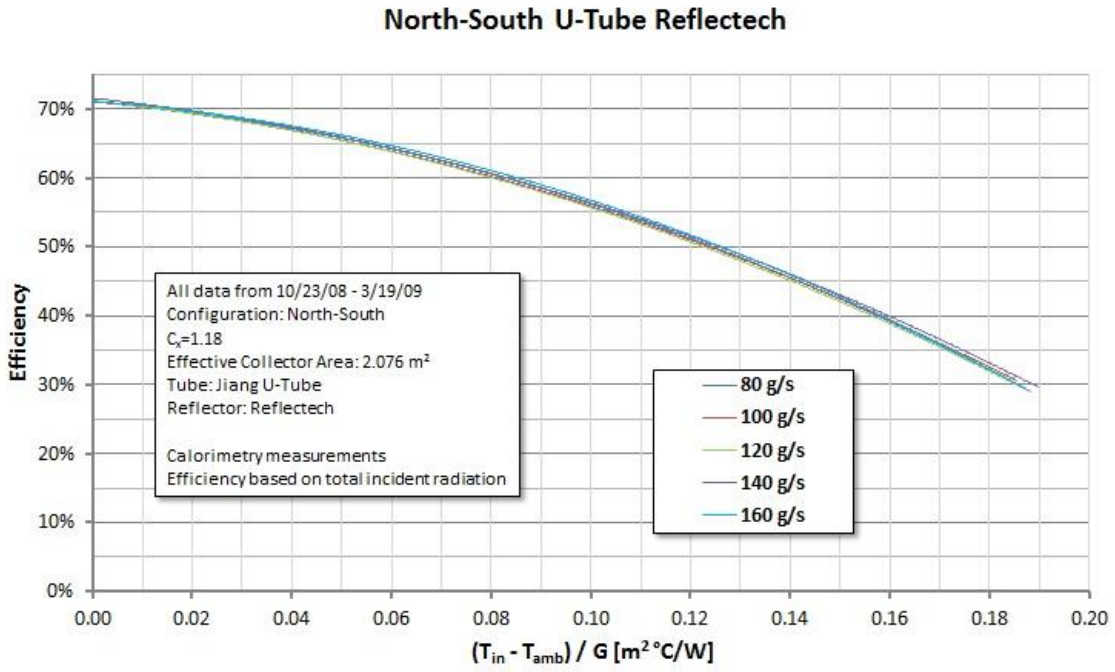

Figure 12 – XCPC Efficiency

The operating performance of the XCPC (as shown in figure X) was measured previously at a separate testing loop at the UC Merced Castle research facility. Most of the work in testing and characterizing the XCPC collector was done by previous graduate student Kevin M. Balkoski. A more detailed description of the design and testing of the XCPC collector can be found in his thesis, "Performance Analysis of Medium Temperature Non-Tracking Solar Thermal Concentrators" [23]. To summarize, several different XCPC designs (East-West vs. North-South orientation, ReflecTech vs. Alanod reflectors, counter-flow tube vs. u-tube) were compared and the best (North-South ReflecTech U-Tube) was selected as the candidate for the current solar cooling project.

It is worth mentioning that the measurement of the collector performance as shown in Fig.4 was done using the calorimetric technique. This simultaneously calibrates both the flow rate and heat capacity of the heat transfer fluid, both of which are prone to variability as the heat transfer fluid degrades over time. The calorimetric technique allows you to calculate the amount of thermal power collected using measurements of temperature and electric power, both of which can be obtained with a high degree of certainty (as opposed to measuring flowrate and assuming a heat capacity and density of the oil).

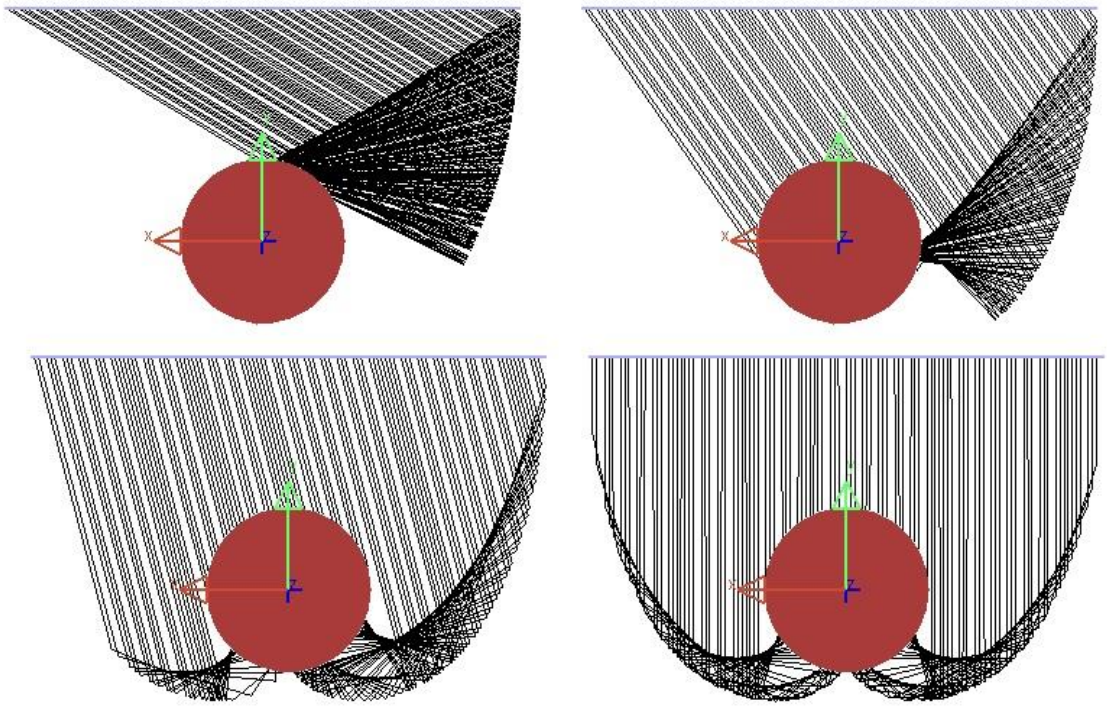

Figure 13 – XCPC Ray Tracing (59°, 45°, 15°, 0°)

The efficiency in Fig. 4 is normalized to total solar radiation using a Precision Spectral Pyranometer (PSP) on the plane of the collectors. If normalized by the direct solar radiation (DNI) as is customary for concentrating collectors, the

efficiencies are *typically* 25% higher. If normalized to C_x corrected radiation, the efficiencies are slightly higher but almost identical (since the concentration is low).

The metal and glass components of the vacuum tubes were sealed using a lead "solder." If the tube gets hot enough (i.e. during stagnation conditions) the lead, which has a melting temperature of approximately 325 °C, can melt and cause the vacuum to be lost. This significantly affects the efficiency of the vacuum tube and causes a net heat loss from the system at temperatures above 140 °C (see Figure 32).

In the interest of preventing this, a stagnation test was performed on a single XCPC collector that was drained of fluid. Temperature inside the vacuum tube reached a maximum of 290 °C in a little over one hour during a sunny day with an average of 1030 W/m^2 global radiation and approximately 20% diffuse fraction and an ambient temperature of 25 °C. Although no damage to the tube was observed, the current XCPC collectors are covered when not in use to prevent any possible damage from long term stagnation. At the writing of this thesis, we also are in the process of installing a solar powered pump as a backup to prevent long term stagnation.

Table 1
Collector Array Specifications

Aperture Area	53.3 m2
Orientation	North-South
Inclination Angle	20 degrees
Concentration	1.18
# of Troughs	160
Evacuated Tube Type	U-tube
Operating Temperature	160-180 °C
Thermal Fluid	Duratherm 600
Thermal Fluid Flowrate	16 gpm

Table 2
Heat Exchanger Specifications

Design Duty	21.9 kW
Fluid 1	Duratherm 600
Fluid 1 Inlet/Outlet Temp	180 / 168 °C
Fluid 1 Flowrate	16 gpm
Fluid 2	Dowtherm 4000 (40% EG)
Fluid 2 Inlet/Outlet Temp	161 / 170°C
Fluid 2 Flowrate	9.8 gpm
Efficiency	0.9

2.2 The Absorption Chiller

The chiller used in this system is a dual fired double effect water and Lithium Bromide (LiBr) absorption chiller rated with a COP of 1.1 for an output of 23 kW (6.6 US tons). It has a natural gas burner in its high temperature generator to provide heat when solar energy is inadequate and a built in cooling tower to reject heat to the environment. It has a nominal power consumption of 1.8 kW which includes all internal components (pumps, controls, ventilation, cooling tower) and uses about 0.25 gpm of water for cooling.

The absorption chiller works by using thermal energy to power an internal cooling cycle. The cycle starts when thermal energy vaporizes water from a dilute solution of water and lithium bromide at high temperatures and pressures in the generator. This water is directed through a second chamber of LiBr + H20 where some of the heat is consumed to drive off even more water vapor, hence the “double” effect. All the water vapor that is driven off is then condensed by rejecting its heat to a cooling water loop in the condenser. The condensate water is pumped into a low pressure chamber causing it to vaporize and absorb heat from a water loop and thus provides a cooling effect. This vaporized water is then re-captured into solution by a

spray of concentrated LiBr in the absorber. The now dilute solution of water and LiBr is then pumped back to the high temperature generator and the cycle repeats (see Fig.14).

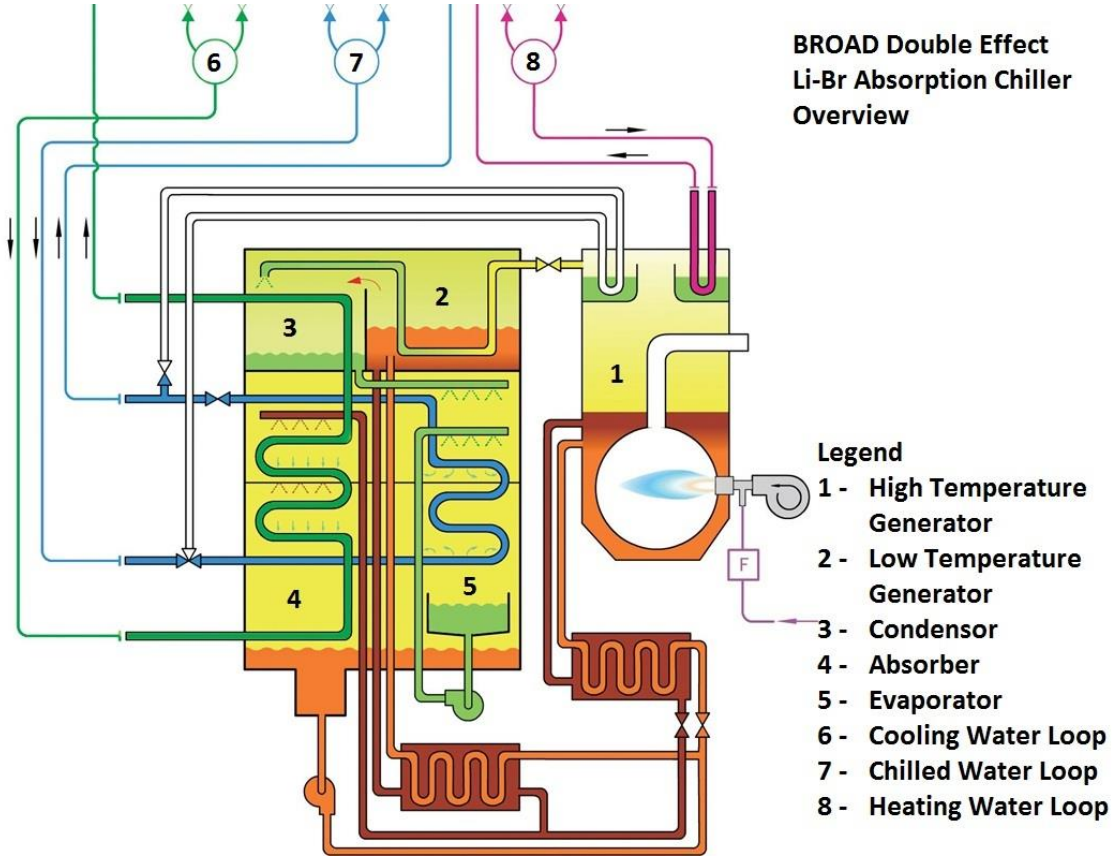

Figure 14 – BROAD Double Effect LiBr + H20 Absorption Chiller Schematic

Table 3
BROAD Micro Chiller (BCTZH23) Specifications

Cooling Capacity	6.6 tons (23 kW)
High Temperature Fluid	Dowtherm 4000 (40% EG)
HTF Inlet	171 °C
HTF Outlet	161 °C
HTF Flowrate	9.8 gpm
Chilled Water Inlet	13.9 °C
Chilled Water Outlet	7.2 °C
Chilled Water Flowrate	13 gpm
COP	1.1
Water Consumption	0.25 gpm
Power (pumps, controls)	1.8 kW

2.3 Sensors and Accuracy

There were a total of 15 sensors installed, including: 2 electromagnetic flow rate sensors (± 1% of reading); one Coriolis Flow Meter (± 0.1 %); 9 T-Type thermocouples (± 0.75% of range); 1 K-Type ambient temperature thermocouple (± 2.2 C); and 1 Precision Spectral Pyranometer (PSP) (± 2.5 %). The measurements collected from these devices were used to characterize system performance.

Thermocouples were placed before and after the collector bank junctions on the oil loop, and mass flow rate was measured by a coriolis flow meter installed after the collector banks. Two thermoucouples were also placed after the heat exchanger and after the chiller on the glycol loop, along with an electromagnetic flow meter. On the water loop, thermocouples were placed at the inlet and outlet of the chilled water line to the chiller and another electromagnetic flow meter was installed at the outlet of the chiller.

The glycol measurements that were made were not consistent, especially with flow measurements (due partly to an ungrounded connection). As a result, glycol measurements were not considered in the analysis due to the inaccuracy of the flow measurements.

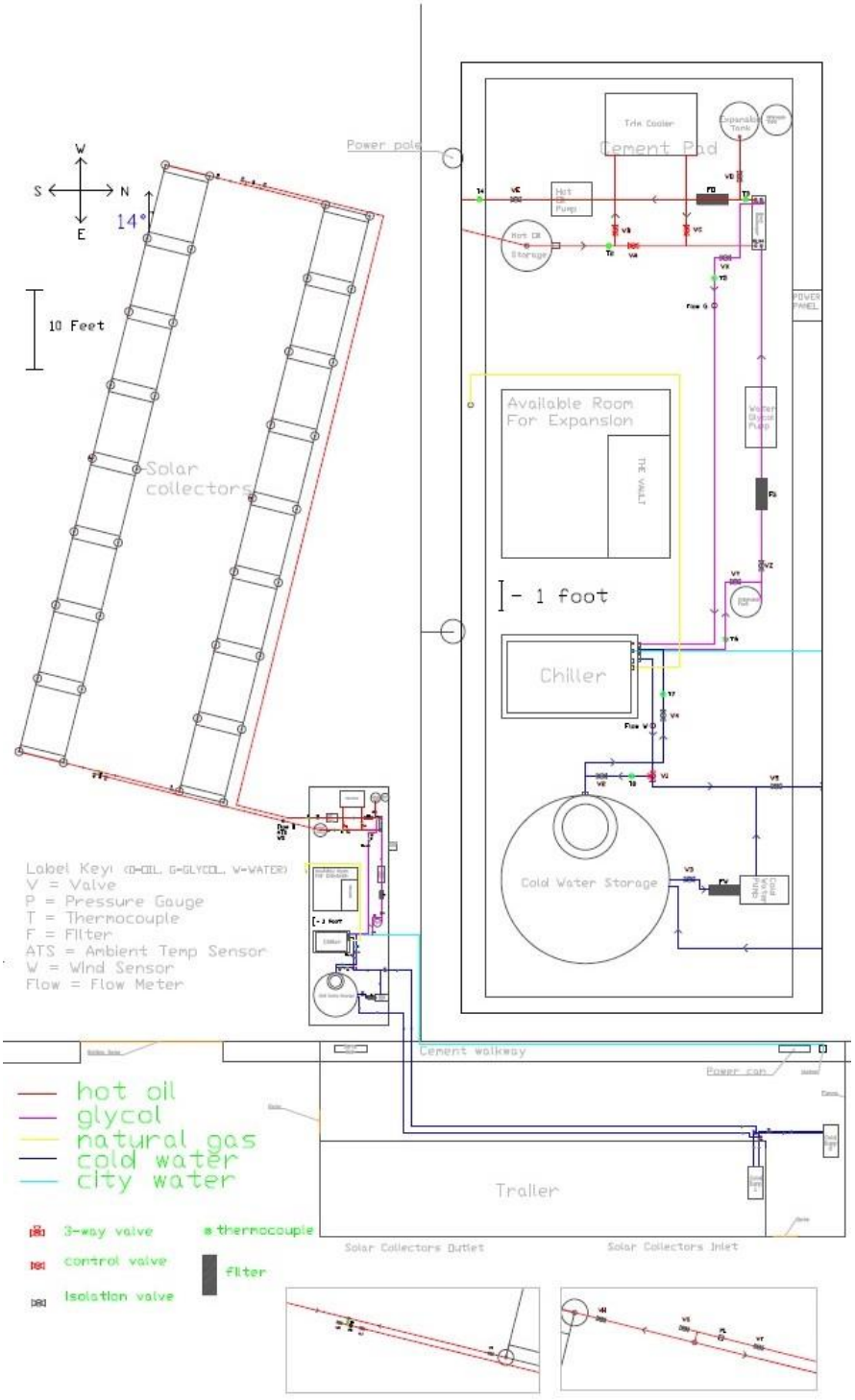

Figure 15 – System Footprint

3. Performance Results

Performance of the cooling system was tested over two weeks in August 2012 and at various times in late summer and early fall of 2011. These tests were performed in both sunny and cloudy conditions, and with clean and dirty collectors to gain an understanding of performance in these cases. Figures 16 and 17 depict a typical day's performance. Figure 16 shows inlet and outlet temperatures for the collectors and chiller (on the chilled water side) as well as the ambient temperature.

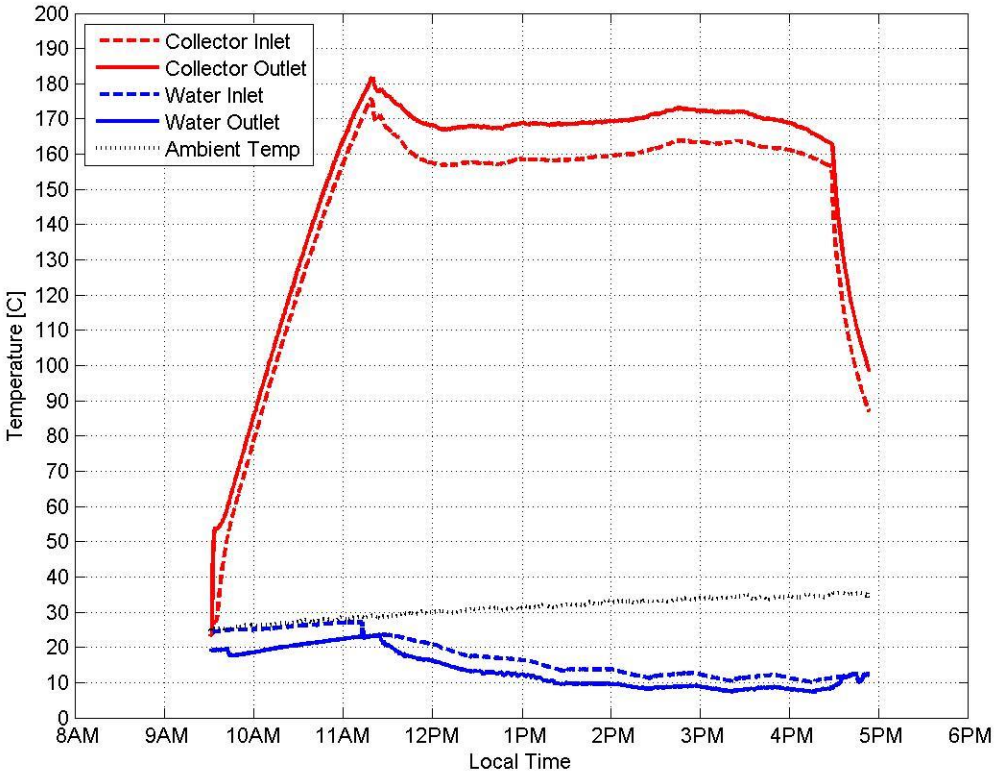

Figure 16 – Aug 22, 2012 – Typical System Performance

Figure 17 shows the corresponding power provided by the sun, the power collected by the XCPCs, and the cooling power of the chiller. The calculated sun power is the product of total collector aperture area and the global tilted solar

irradiation (GTI), provided by a PSP sensor mounted at the same inclination as the collectors on the collector frame (thus including the cosine effect). Oil power (thermal) is calculated as the product of the flow rate, heat capacity, and temperature difference across the collectors. Cooling water power is calculated as the product of the water flow rate and the temperature difference of the chilled water over the chiller. Glycol power typically followed, but was 1-2 kW lower than the water power output from the chiller. The glycol outlet temperature from the heat exchanger was typically the same as the inlet temperature to the collectors. The time step for data collection was 10 seconds.

3.1 Performance Tests

During these tests, the collector and intermediate glycol loops were circulated for about two hours until the temperature was high enough to drive the double effect absorption chiller. Then a bypass valve was switched so that the high temperature glycol passed through the chiller and provided thermal power to drive the absorption cycle. No natural gas was used to power the chiller during these tests and as a result, there is a delay between when the collectors start losing temperature and when the chiller starts producing cooling. This is due to the time it takes for the thermal fluid to warm up the high temperature generator inside the chiller from ambient temperature to the required temperature.

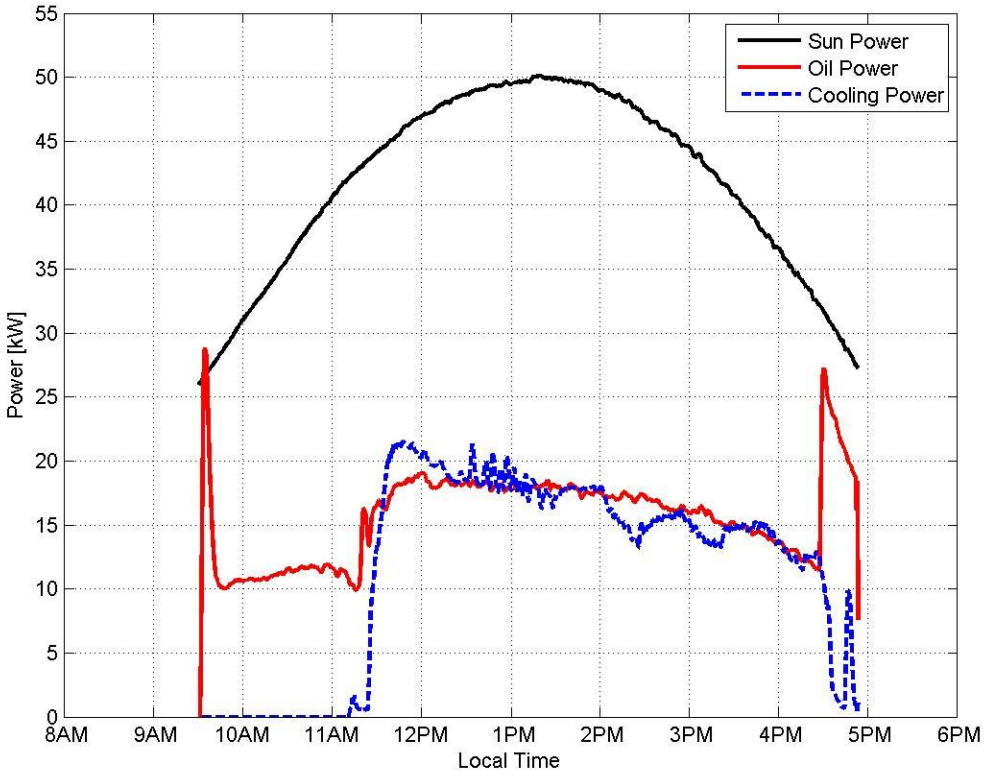

Figure 17 – Aug 22, 2012 – Typical System Performance

As the system runs, the chiller cools water from a 500 gallon storage tank. Water from this tank is circulated into an air handling unit that absorbs heat from inside the trailer. This acts as the cooling load on the chiller but during our tests was not enough to match the cooling power provided by the chiller. As a result, temperatures in the cold water tank decreased until they reached the minimum outlet temperature of the chiller (6 °C). This had the effect of decreasing the chiller's COP later in the day because it becomes increasingly more difficult for the chiller to cool water that is already cold [21]. Once the cold water inlet temperature reaches the minimum limit of the chiller, the chiller cycles off for a short period of time to allow the chilled water to warm up. This cycling can be seen in Fig. 16. When the

chiller cycles off, no thermal energy is removed from the high temperature fluids, causing temperatures in these loops to increase. This became an issue in the intermediate glycol loop where high enough temperatures sometimes caused the water in the loop to vaporize which created enough pressure to stop the pump. The system was shut down when either the temperature in the intermediate glycol loop became too high or the solar input became too low. Then the high temperature fluids were circulated through a trim cooler until the temperatures dropped below 100 °C and the solar input dropped below 600 W/m^2.

The expected solar COP of the system can be estimated according to Eq. (7) as the product of the efficiency of the collectors, efficiency of heat transfer from the collectors to the chiller, and the COP of the chiller.

$$Esimated\ COP_{Solar} = \eta_{col} * \eta_{thermal} * COP_{chiller} \quad (7)$$

Using a value of 45% for the collector efficiency based on operating temperatures around 170 °C and an ambient temperature of 30 °C and assuming a thermal efficiency of 0.9 (10% of heat captured by collectors is lost on its way to the chiller), the estimated solar COP of the system is approximately 0.45. We can rewrite the thermal COP in terms of its components. Thus our estimated thermal COP is approximately 0.99.

$$COP_{thermal} = \eta_{thermal} * COP_{chiller} \quad (8)$$

3.2 Typical Performance

Daily values for the collector efficiency, thermal COP, and solar COP of the system were calculated from the time the chiller began producing cooling until the system was shut down. For the typical performance day (Fig. 16,17), this

corresponded to the time period from 11:45 am to 4:20 pm. Daily collector efficiency was determined according to Eq. (2), by integrating the collector power and dividing by the integral of available solar power over the operational time period. The daily thermal COP was calculated according to Eq. (3) by integrating the cooling power and dividing by the integral of collector power over the operational time period. The total solar COP of the system was calculating according to Eq. (4), by integrating the cooling power and dividing by the integral of available solar power over the operational time period.

When the collectors were operated between 150-180 °C, they reached instantaneous efficiencies between 34% and 40%. The instantaneous thermal COP and solar COP ranged from 0.769-1.181 and 0.278-0.468 respectively. The maximum output of the absorption chiller was about 22 kW although on average it produced 15-20 kW of cooling.

Table 4 Results and Definitions – Typical System Performance		Range (Instantaneous)	Daily Average
Collector Efficiency	Thermal power captured per available solar power	34.5%-40.6%	36.7%
Thermal COP	Cooling power per captured collector power	0.769-1.181	0.990
Solar COP	Cooling power per available solar power	0.278-0.468	0.363

Values for collector efficiencies were somewhat lower than expected. This is likely caused by heat loss in the collector array between the temperature sensors used to measure the ΔT_{col}. Since this was an educational project, the collectors were ground mounted and not optimally spaced, requiring more pipe length in the collector array than anywhere else in the system. A complex manifold configuration along the collector banks (supply and return piping runs, perpendicular vacuum

tube connections, and flexible hoses every 10 tubes to accommodate thermal expansion) made it difficult to insulate all surfaces effectively.

These limitations would be mitigated in a commercial system where piping runs are minimized and optimally insulated. A discussion on other causes for heat loss in the collector array is presented later. The calculated thermal COP, however, is in good agreement with the expected thermal COP.

3.3 Cloudy Day Performance

Performance of the system was also measured on two cloudy days. Due to the optics of the design, the XCPC collector can collect a certain fraction of diffuse light (1 / concentration). The collectors used in this system had a concentration ratio of 1.18 and thus were able to collect 87% of diffuse light. This allows them to collect power on certain types of cloudy days. Obviously no type of solar collector will work well on an entirely overcast day but the XCPC, and other non-tracking collectors such as flat plates, are still able to collect power. This is especially true on days where clouds are interspersed with sunshine because clouds act as giant mirrors, amplifying the amount of diffuse light just before crossing the sun (see Fig. 19), and a solar collector which accepts diffuse light can take advantage of this effect.

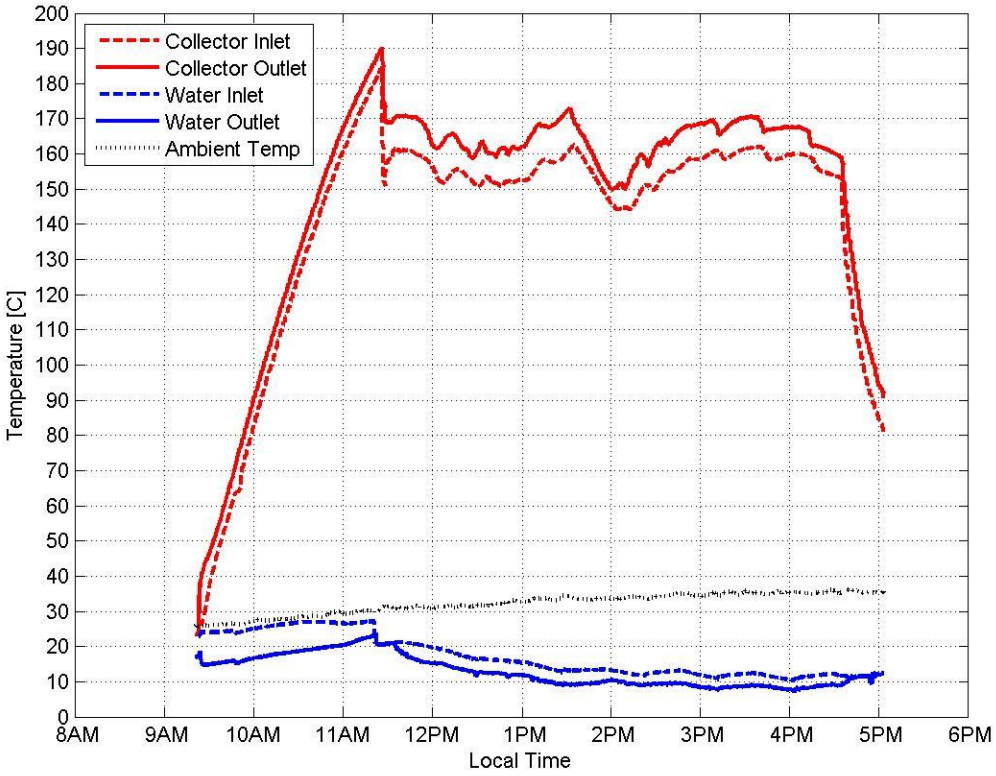

Figure 18 – Aug 21, 2012 – System Performance under Cloudy Conditions

The system was run in the same manner on cloudy days as on clear days and no natural gas was used to power the chiller. While it is difficult to provide typical data for a cloudy day because of the wide variability of cloud cover with time of year and location, the data shown in Fig. 18 and 19 is promising because the collectors were still able to maintain temperatures above 140 °C and an appreciable amount cooling was still being produced. It is also important to take note that on cloudy days there is usually less of a need for space cooling and thus a decreased cooling output may in some cases be completely acceptable. Collector efficiency, thermal COP, and solar COP were calculated as before for an operational time period between 11:40 am and 4:30 pm and the results are presented in table 5. Instantaneous values are

presented, but should be regarded with an understanding that the high variability of solar insolation and the latency of response in the temperature sensors cause inaccurate calculations on an instantaneous basis. They are included simply for completeness.

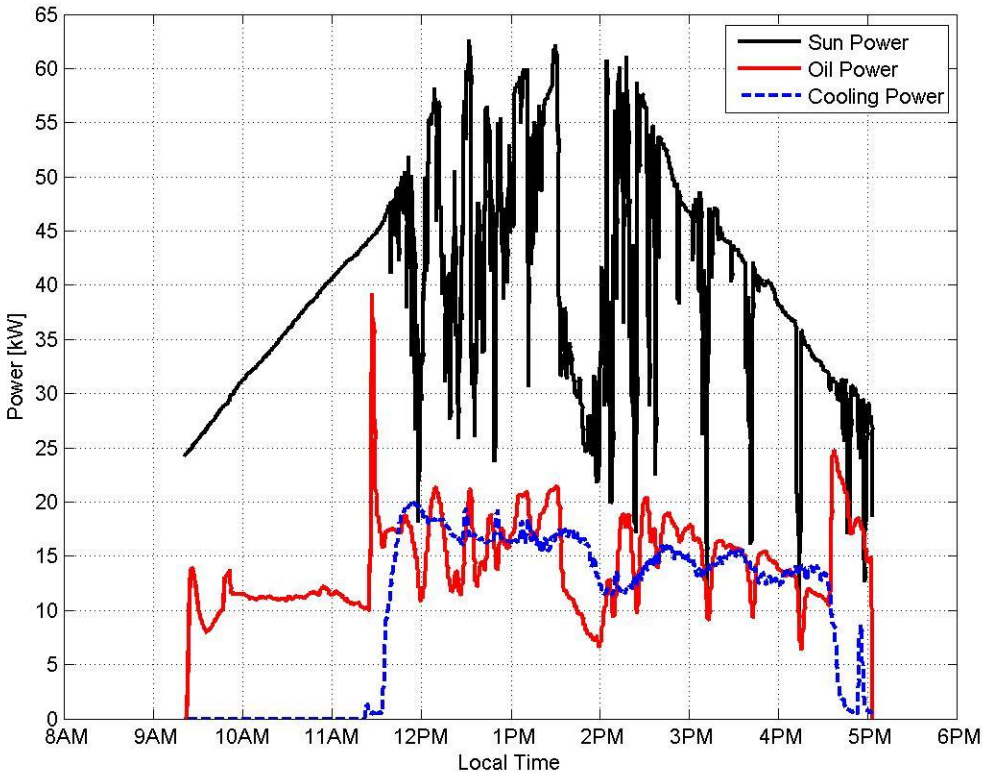

Figure 19 – Aug 21, 2012 – System Performance under Cloudy Conditions

Table 5 Results and Definitions – Cloudy Day Performance		Range (Instantaneous)	Daily Average
Collector Efficiency	Thermal power captured per available solar power	19.6%-64.1%	35.5%
Thermal COP	Cooling power per captured collector power	0.617-2.236	1.019
Solar COP	Cooling power per available solar power	0.204-0.886	0.362

3.4 Collector Cleaning

The efficiency of the solar collectors is directly affected by the amount of dust that has settled on the reflectors and vacuum tubes. Over time, the accumulation of dust particles that absorb and scatter sunlight decreases the efficiency of the collectors. The rate of accumulation depends on a variety of environmental factors tied to the location of the array such as wind speed, vegetation, proximity to farmland, and climate. The solar array used in this cooling demonstration was built next to a vacant plot of land and an orchard. Prior to taking data, the collectors had not been cleaned for almost a year, the plot of land next to the collectors was razed of vegetation, and the orchard was razed and re-planted with new trees. As a result, the collectors themselves were extremely dirty and the data probably represents a worst case scenario. Testing was performed for 4 days with dirty collectors and then for 4 days after cleaning the collectors. Prior to cleaning, the collectors operated with an average daily efficiency (according to each day's specific operational time period) of 30% and after cleaning operated with average daily efficiencies of 36.9%.

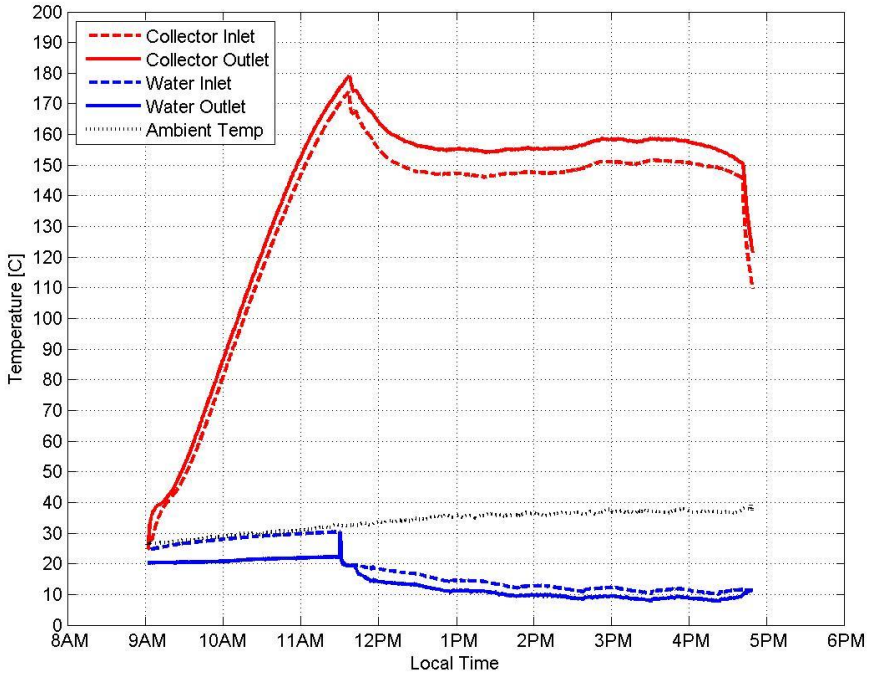

Figure 20 – Aug 15, 2012 – System Performance with Dirty Collectors

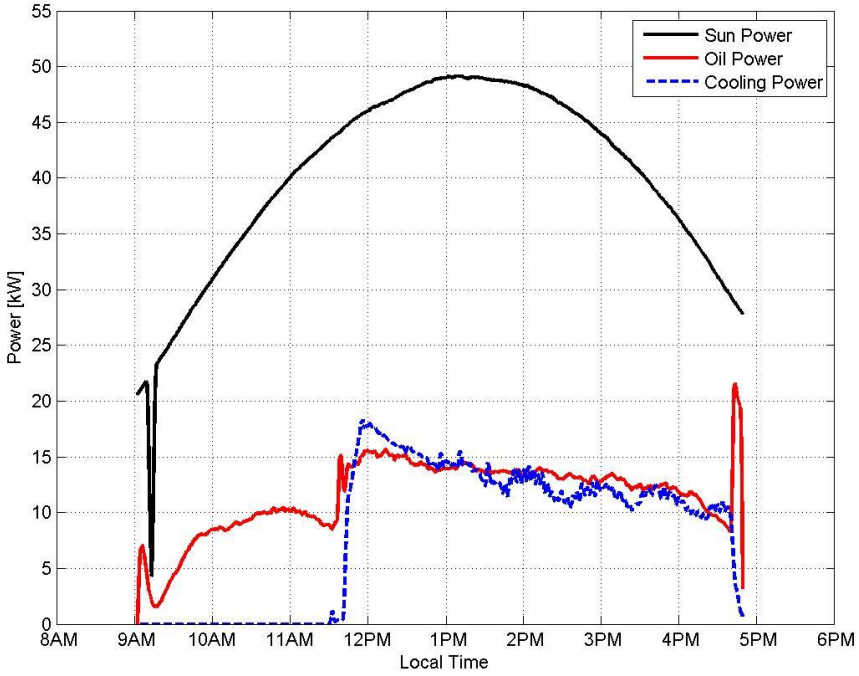

Figure 21 – Aug 15, 2012 – System Performance with Dirty Collectors

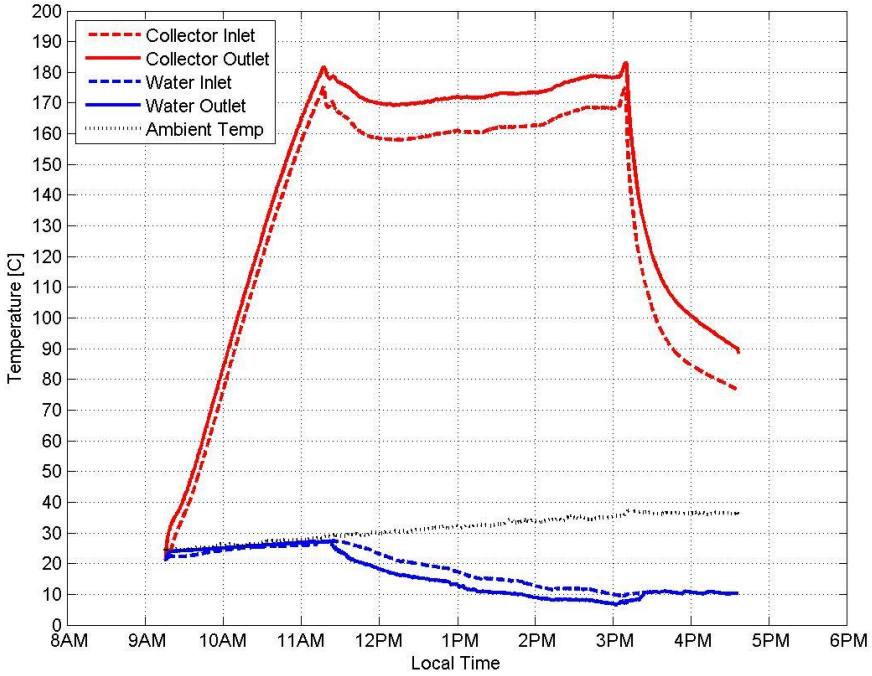

Figure 22 – Aug 20, 2012 – System Performance with Clean Collectors

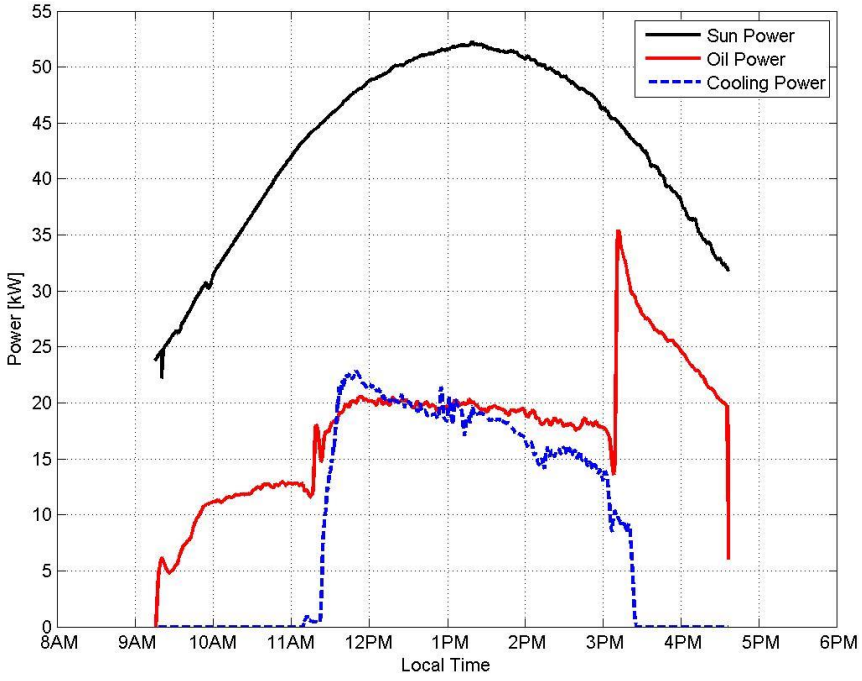

Figure 23 – Aug 20, 2012 – System Performance with Clean Collectors

Figures 20 and 21 present data from a day when the collectors were dirty, and Fig. 22 and 23 present data after they were cleaned. On August 15th (dirty collectors) the system was run for a full 8 hours while on August 20th (clean collectors) the system was run for about 6½ hours. The difference is run time was caused by our low cooling load. When the collectors are dirty, they capture less power, maintain lower temperatures and do not provide enough cooling to overpower our cooling load. As a result we were able to demonstrate the full 8 hour solar collection window (2½ hours warm-up, 5½ hours run-time). However, once the collectors were cleaned, they warmed up 30 minutes faster, maintained much higher temperatures, and quickly overpowered our cooling load causing a low chiller COP and chiller cycling (Fig. 23). As mentioned before, this forced us to shut down the system due to risk of vaporization in our intermediate water-glycol loop. Our inability to run for a full 8 hours with clean collectors was simply due to our undersized cooling load and would not be an issue in a properly sized system.

3.5 Warm-up Time

The warm-up time of the system is directly related to the total mass of piping, valves, pumps, and fluid that need to be heated from ambient to operating temperatures. In 2011 (first cooling season), the system included a large 50 gallon thermal storage tank with the purpose of evening out fluctuations in solar radiation. This greatly increased the total mass of fluid in the system and increased the system warm up time by approximately 1 hour (see Fig. 24, 25). Because the collectors have an 8 hour collection window, any increase in warm up time cuts into power production time and should be minimized. Therefore it is important to design a

system with a small heat capacity in the high temperature loops by minimizing pipe diameters, lengths, and fluid volume.

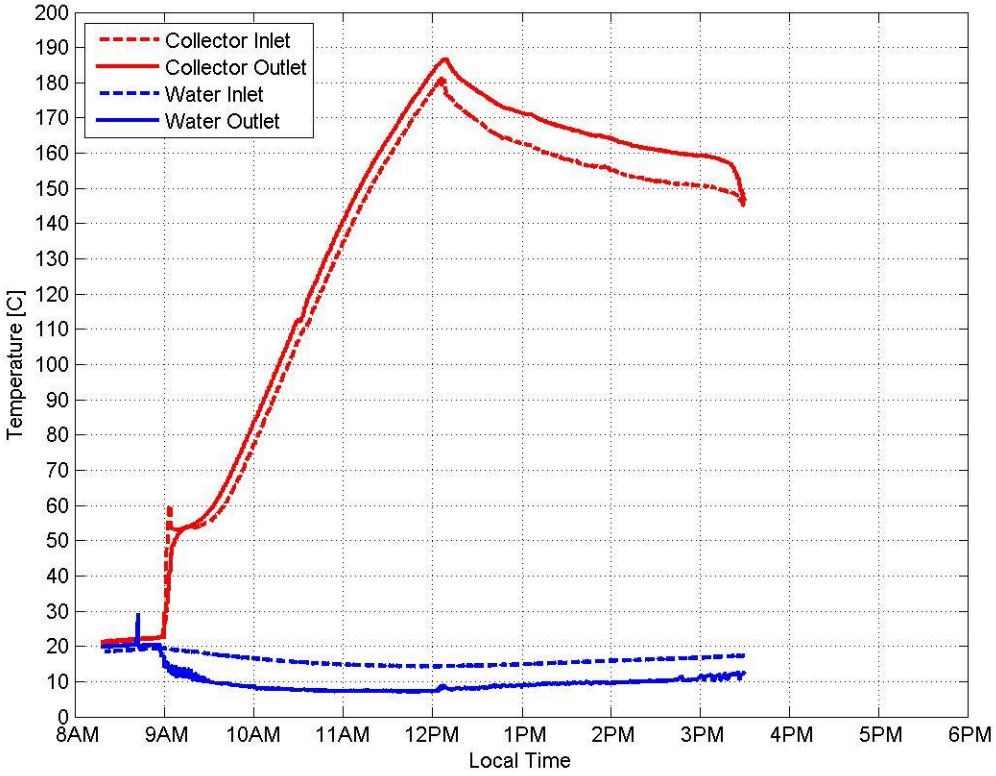

Figure 24 – Sept 23, 2011 – System Performance with 50 gallon Storage Tank and Natural Gas powered Chiller

During the 2011 tests, the chiller was powered by natural gas during the system warm up period and then switched to solar power once operating temperatures were reached. As a result, we were able to demonstrate the benefits of a hybrid solar powered cooling system by producing a seamless output of cooling power from both natural gas and solar power inputs. Also during these tests, the air handling unit on the chilled water loop was not connected to the trailer, but was instead dumping cooling power to the outdoors. This acted as a much larger load on the chiller and prevented the chilled water loop from reaching temperatures close to

the minimum allowed by the chiller. As a result, we were able to maintain a much more stable cooling output and chiller COP.

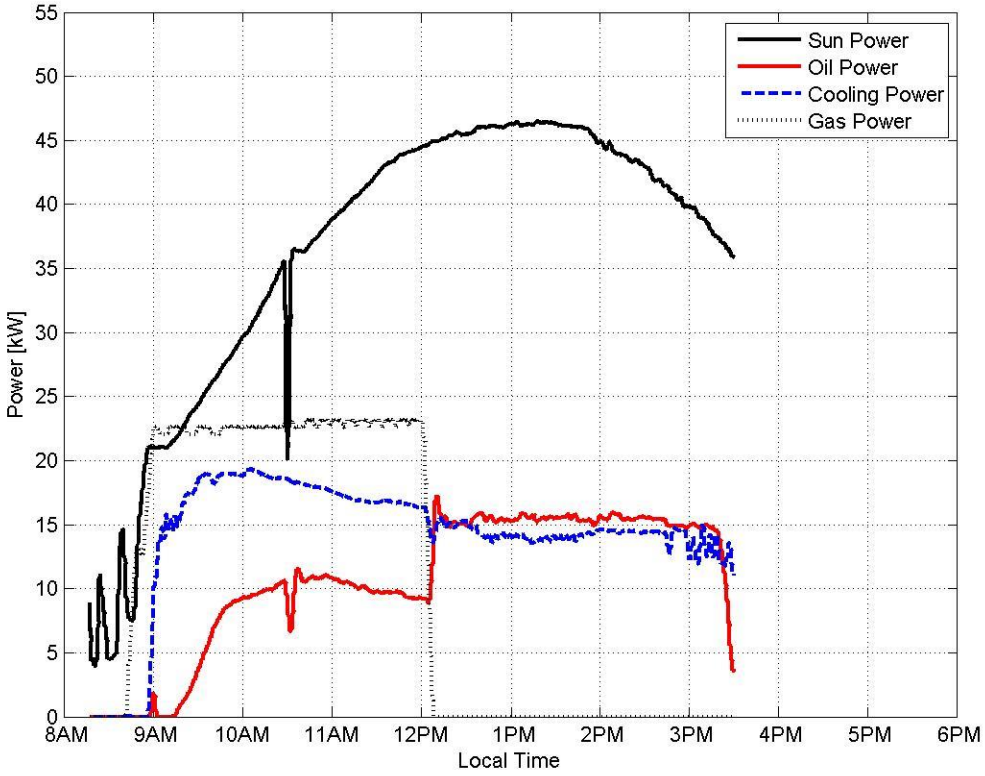

Figure 25 – Sept 23, 2011 – System Performance with 50 gallon Storage Tank and Natural Gas powered Chiller

3.6 Cooling Window

The XCPCs collect solar energy for 8 hours out of the day. With an average warm up time of 2 hours, this leaves 6 hours of direct solar powered cooling. Depending on the location this is approximately from 11 am to 5 pm. However, the typical cooling load lags behind the available solar energy by a couple of hours and in some locations, space cooling may be needed before or after the direct solar powered cooling window. Typical Meteorological Year (TMY) Data was used to determine hourly cooling needs throughout the year for Merced, CA. A hybrid chiller

can provide cooling from natural gas in the morning during the warm up time of the collectors (see Fig. 24, 25) and cold storage can lengthen the cooling window into the late afternoon and evening. The use of cold storage is recommended over hot storage due to a smaller temperature difference with the ambient and therefore less heat loss (or gain). An oversized collector array can provide direct solar powered cooling while also cooling a water storage tank. When the system no longer collects solar power, the cooled storage tank can then be circulated to provide additional cooling into the evening. The storage tank and collector array can be sized to provide the required duration of cooling.

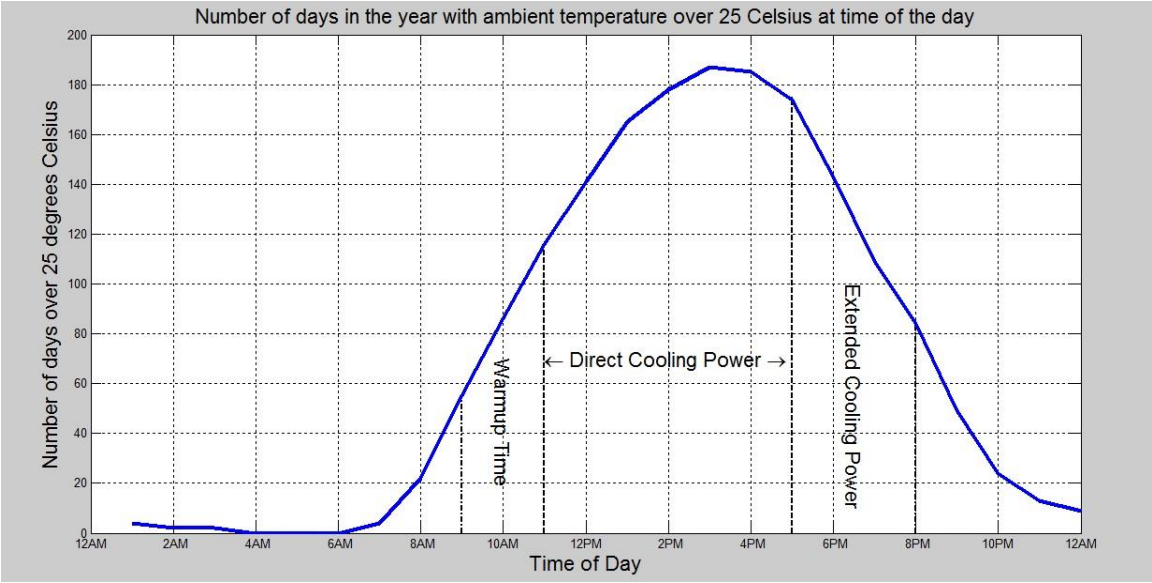

Figure 26 – Hourly cooling needs in Merced, California based on TMY data

3.7 Electrical Power Consumption and Parasitic Loss

Parasitic losses occur due to the fact that it takes power (pumps, chiller, fans) to produce cooling power in a solar cooling system. None of the electrical components in the system were monitored for electrical consumption, but a rough estimate of can

be calculated based on the rated power consumption for the important components and their operating capacities. The parasitic solar COP is calculated according to Eq. (5). For the typical system performance day (Aug 22, 2012), the chiller produced an average of 16.25 kW cooling, corresponding to a cooling capacity of 70% and an electrical consumption of 80% [21] of the rated power. The collector pump (1.5 HP) was oversized and at our flow rate and pressure operated at 63% capacity. The solar cooling system produced 76 kWh of cooling from 209 kWh of available solar energy over the operational time period. Total electrical consumption was calculated accounting for a 2 hour warm-up period during which the collector pump was running, and for a 5 hour operational period of the chiller and collector pump, and totaled at 12.17 kWh. None of the actual electrical usage was measured and this is only provided as a rough estimate of electrical performance of the system. It is worth mentioning here that an electrical COP of 6.25 is fairly high, and comparable to large vapor compression chillers. A solar cooling system, however, will cost much more initially than a vapor compression chiller, and thus the electrical COP must be much higher (in the range of 10) to become a more attractive option. This is not out of reach, especially with improvements such as using a solar powered pump.

Table 6 – Electrical Consumption

Operational Solar (kWh)	Available Solar Energy during operational period	209.06
Operational Cooling (kWh)	Cooling Produced during operational period	75.98
Total Electrical (kWh)	Total electrical consumption	12.17
Solar COP (thermal)	Solar COP considering only thermal terms	0.36
Solar COP (parasitic)	Solar COP including parasitic losses	0.34
Electrical COP	Cooling produced per electricity consumed	6.25

3.8 Economic Evaluation

A simple economic evaluation of the system was performed using commercially available materials. Excluding the chiller, the most expensive components were the metal-glass evacuated tubes, the collector frame (that holds the XCPCS in position), and manifolds (evacuated tube to piping connections).

For this demonstration project, the XCPC reflectors were molded out of plastic and lined with a reflective film by hand. This is not an economic approach and would not be the method of choice for a commercially produced system. Reflector price was estimated for a polished aluminum that is bent into the required XCPC shape by a machine. The total cost per square meter of the XCPC collector system, including piping, insulation, pumps, and other miscellaneous equipment often referred to as the balance of system, came to be about $\$270/m^2$. For an average insolation of 1000 W/m^2 and collector efficiency of approximately 37% (as achieved by this demonstration project) the cost of the collectors and balance of system is about $0.72/watt. Prices for double effect absorption chillers range from $400/kW to

$1000/kW depending on the size. The target investment price, based on a large system to make the absorption chiller price more economical, is approximately $1.12/watt.

Table 7 – Price Estimation	Cost per square meter ($/m^2)
Reflector	18.27
Frame	75.00
Manifold	40.32
Fluid	11.00
Tubes	75.48
Manifold Insulation	5.68
Collector Module	225.75
Pumps	4.16
Pipe	4.58
Pipe insulation	2.92
Valves	2.67
Controls	1.00
Miscellaneous Balance of System	2.00
Engineering	14.26
Installation	12.27
System Total	269.61

4. A Discussion on Maintenance, Obstacles, and Recommendations

After running the system for two cooling seasons, we have faced a number of obstacles and identified certain system design aspects that can be improved for future installations.

4.1 Intermediate Glycol Loop

The first is the issue of the intermediate glycol loop. This loop was installed for no reason except to separate the chiller from the mineral oil in the collector loop. The glycol pump was able to provide a maximum pressure head of 140 psi. When the fluid in this loop reached temperatures above 180 °C, however, the vapor pressure of

the fluid passed 140 psi and effectively stopped the pump from pumping. This forced a shutdown of the system on a number of occasions. We are now in the process of removing this loop and extending our oil loop into the chiller. This will simplify system operation (fewer loops to manage, pumps), reduce heat loss (no heat exchanger), and eliminate the overheating problem we have encountered these past two years.

4.2 Cooling Load

A second obstacle that we faced was an inadequate cooling load caused by a poor HVAC design (this occurred only in the 2012 tests). In 2011, the trailer was cooled by pumping cold water from the storage tank through a coil installed in-line with the ducting of the existing mounted A/C unit (Bard Wall-Mount). After the water passed through this coil, it was directed to an external blower (fan and coil) that exhausted cooling to the environment before being returned to the cold water storage tank. The combination of these two cold sinks and the fact that the cold water tank and much of the cold water loop was un-insulated provided enough load on the chiller for it to run continuously. The trailer, however, never became exceedingly cold due to the fact that the fan in the existing mounted A/C unit did not provide enough CFM for the in-line coil to effectively chill the entire trailer (especially the rooms furthest away).

In an attempt to remedy this, the input and output of the external Carrier blower was connected to the trailer for the 2012 tests and cooling was exhausted into the trailer rather than the environment. While this did indeed make the trailer cooler to work in (but still not as cold as we would have liked), less cooling was removed from the cold water loop because there was a much smaller temperature

difference between the cooling air from the trailer and the cooling water. As a result, the cold water in this loop decreased until it reached the minimum outlet temperature of the chiller (as described previously) and caused chiller cycling.

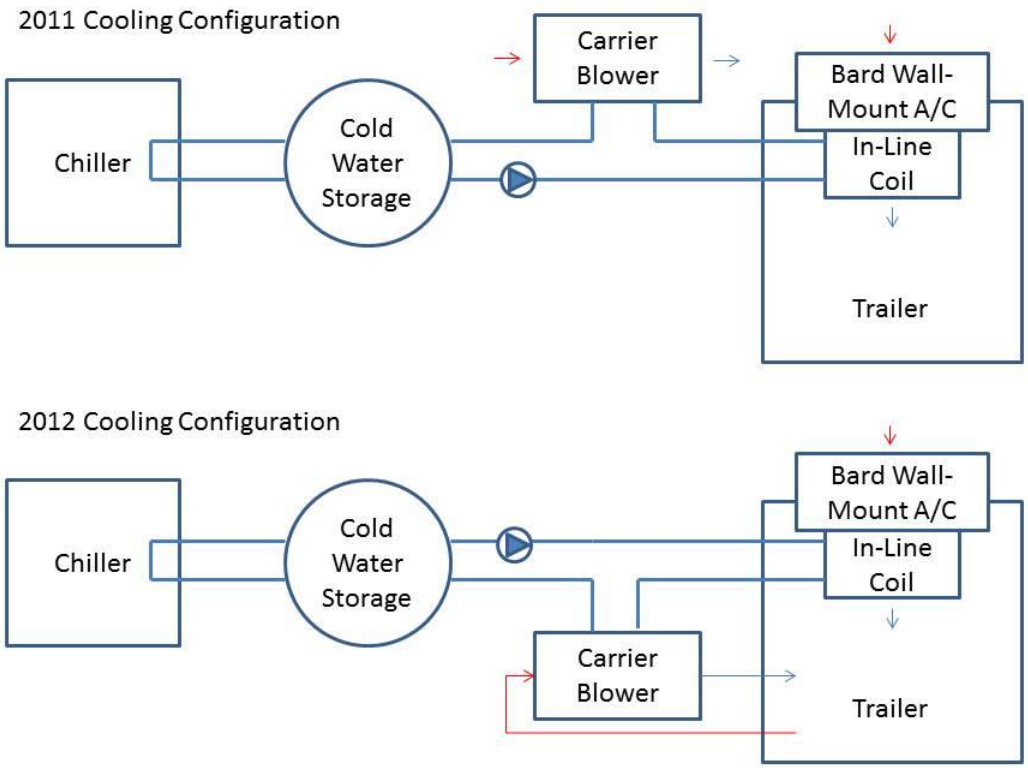

Figure 27 – Cooling Loop Configurations

Table 8 - Cooling Capacities

	Capacity (Tons)	CFM
BROAD Chiller	6.6	
Bard Wall-Mount		800-1000
In-Line Coil	2.3	1200 (req'd)
Carrier Blower	1.5	800
Total Cooling Load	3.8	

The solution to this is to provide enough cooling load to balance the cooling provided by the chiller. Since the trailer is undersized for our cooling load, a cold

dump (such as our Carrier blower) is always necessary to exhaust the extra cooling. Ultimately, this is a simple HVAC problem that was not properly addressed (due to budgetary concerns) and unfortunately had a significant effect in the operation of the cooling system.

4.3 Vacuum Tube to Manifold Connection Leakage

The third and probably most significant problem we have faced is the issue of oil leakage from the vacuum tube to manifold connections. As oil leaks out of these connections, it soaks into the insulation, reducing its effectiveness and increasing heat loss (as the insulation basically assumes the thermal conductivity of the oil).

Figure 28 – Insulation damage from oil leaks

This increases maintenance costs as insulation and oil must be replaced and presents a potential fire safety hazard. The metal to metal flare fitting (between the

vacuum tubes and manifolds) was chosen because it is one of the most secure type of connections. There are, however, a number of factors that cause it to fail.

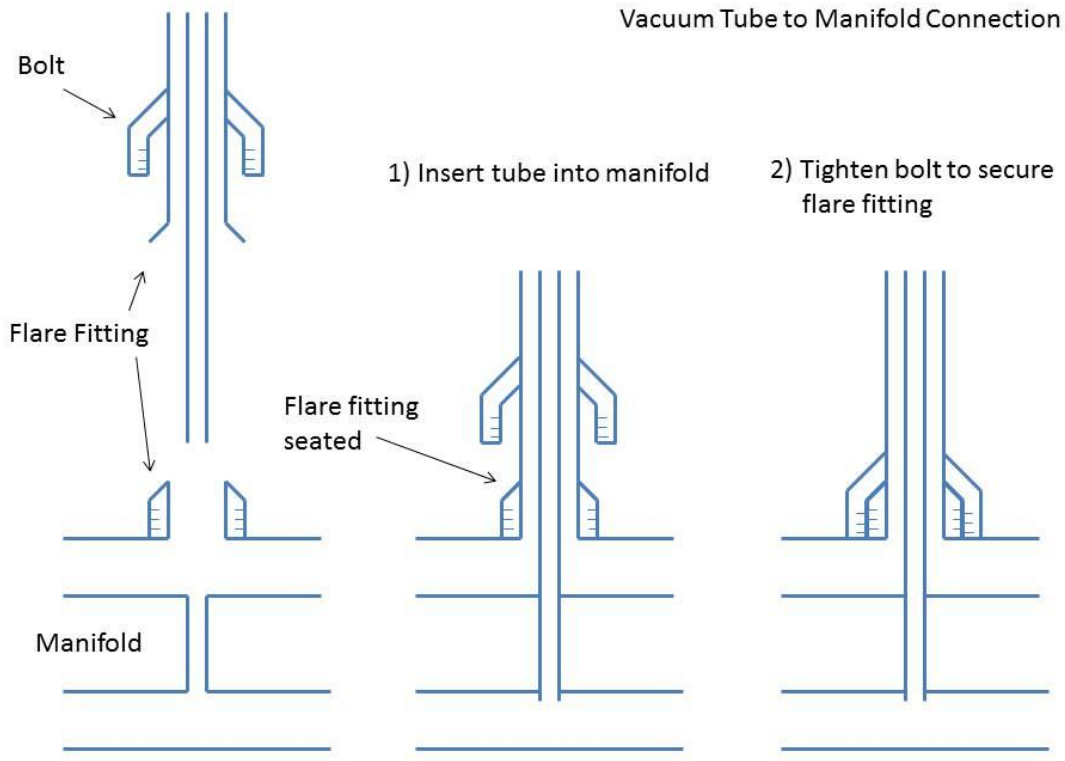

Figure 29 – Vacuum Tube to Manifold Connection

Each time the system is run, the copper manifolds and tubes and the brass flare fitting connections experience thermal expansion as the system heats up and a contraction as it cools down. This cycling contributes to a slow un-screwing of the bolts (a large number of bolt fittings were loose after 2 seasons). The connection is also at an angle, which increases the complexity of aligning the flare fitting and increases the chances that it will deform in an irregular way. The connection is also load bearing (supports the vacuum tubes) and the flare itself is made of copper which is soft enough to deform easily especially when exacerbated by the conditions

listed above. Once the flare becomes deformed, it is difficult to align it back so that it seals completely.

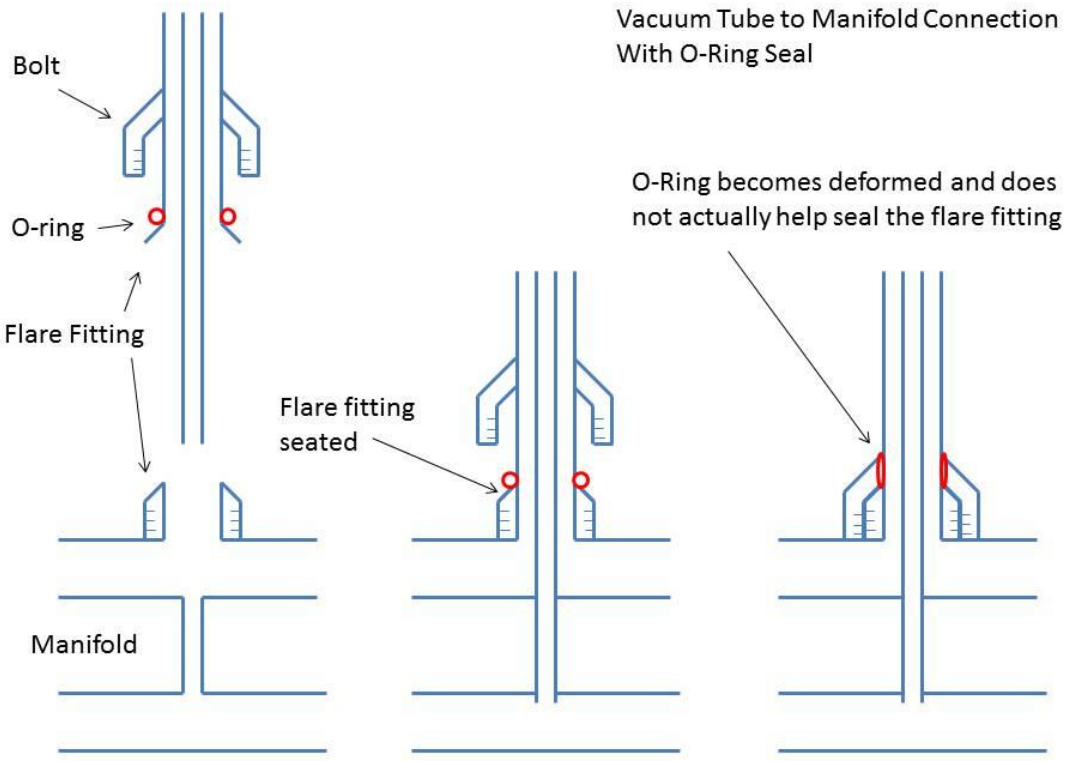

Figure 30 – Vacuum Tube to Manifold Connection (O-Ring)

In 2011, the vacuum tubes were installed with an O-ring placed above the flare fitting. Unfortunately the O-rings were not in the correct position to seal a flare fitting (and in fact should never have been used at all). Over time the O-rings became stiff and disfigured and basically ineffective (we have since removed them all). We are currently in the process of solving the problem of leaks. One potential solution is to simply use heat pipes. Heat pipes have the benefit of not requiring a liquid to flow through them (making it incredibly easy to replace broken tubes and perform maintenance on the system), but have a much lower heat transfer between

the tube to the fluid inside the manifold (low fin efficiency). A second potential solution is to weld or sweat-solder the connection between the vacuum tube and the manifold. This will ensure that there are no leaks, but if a vacuum tube breaks there is no way to easily fix it. You must also be careful when performing the soldering to not overheat the metal-glass seal, which is made of lead and will melt at 300 °C. The last option we came up with was to use a metal washer (built with the same angle as the flare fitting) to basically extend the flare. This would allow us to get a tighter seal by providing more threading with which to tighten the bolts. Since we were not prepared to accept a significant reduction in efficiency using heat pipes, and were not yet committed enough to weld all the tubes to the manifolds, we chose the third option and after the summer 2012 tests installed these washers on every single tube.

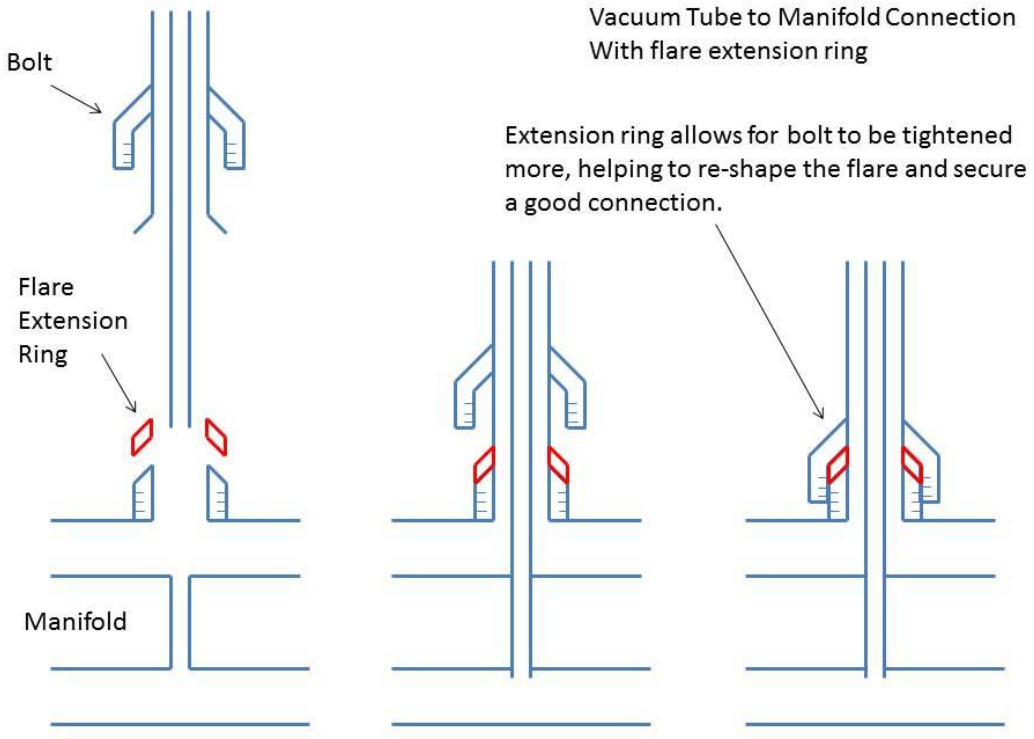

Figure 31 - Vacuum Tube to Manifold Connection (Flare Extension Ring)

While they seem to be working (no leaks for a whole winter season), they require additional and long term testing as we have yet to perform any high temperature tests with them (coming this summer 2013).

4.4 Component Durability

After being run for two cooling seasons and sitting in the elements for almost 4 years, it is worth commenting on the durability of components in the system. I am pleased to report that the plastic reflectors and the ReflecTech, which is attached to the troughs with only the adhesive that came with it and sealed on the edges using an aluminum tape, has held up surprisingly well. There is no visible degradation of the shape or mirrors, except for the accumulation of dust. The manifolds, however, which are held only at each end of the collectors have visibly deformed and are bowed in the middle due to the weight of the vacuum tubes. This may have been a contributing factor in the development of leaks in the manifold to vacuum tube connections and can potentially be solved by a number of different solutions. The first is to switch the placement of the manifolds so that they rest at the top of the collectors. Then, a tube support strip can be placed at the bottom of the collectors (where the current manifolds are) to gently hold the vacuum tubes against gravity. The only problem with this modification is that the tubes will not drain of oil when they are detached from the system. Another potential solution that we are currently investigating is to support the manifold with rigid insulation inside a pre-fabricated box. This will have the benefit of cleaning up and protecting the insulation, making the system look professional, and providing a structural support for the manifold.

4.5 Vacuum Tube Lifetime

Lastly, there are a concerning number of vacuum tubes that are beginning to lose vacuum. This is determined both by hand measurements (touching the tube during operation) and by a visible blackening (oxidation) of the barium getter inside the evacuated tube. After two cooling seasons, 8 tubes have lost vacuum (and have been replaced) but a significant number are on their way. The purpose of the evacuated portion of the tube is to eliminate heat transfer via convection from the hot metal absorber to the cool glass tube. Once the vacuum is gone, heat loss from the tube becomes linear with temperature (as convection dominates), causing a net loss of heat from the tube at temperatures above 140 °C.

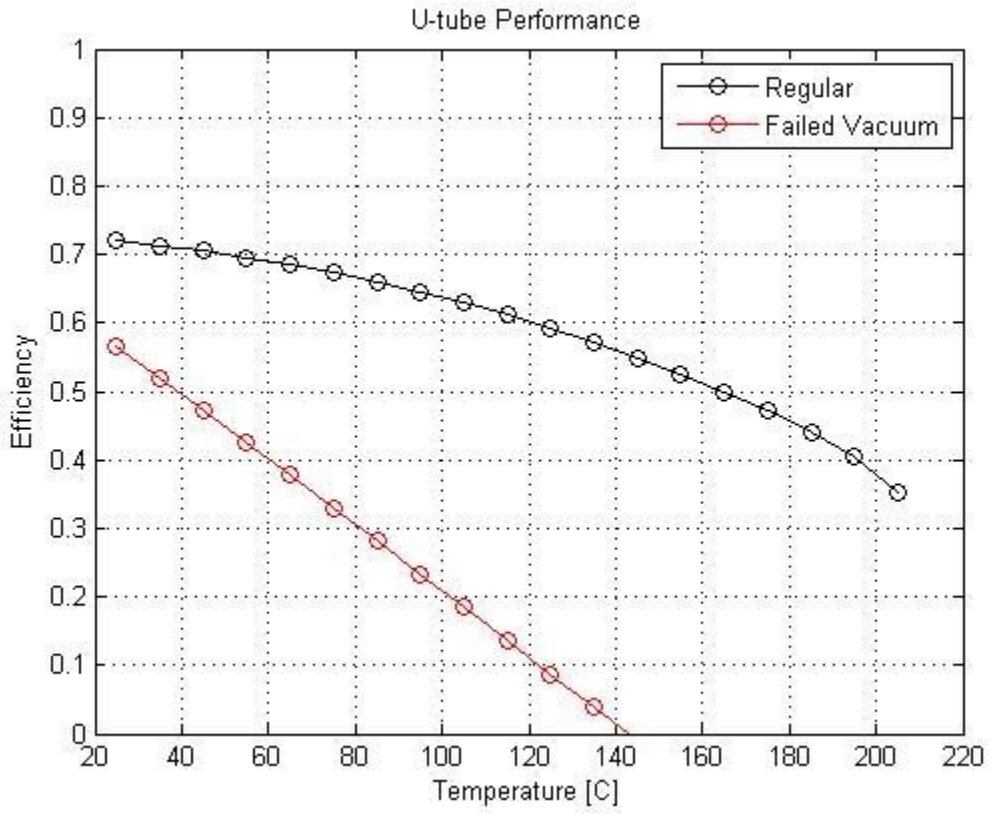

Figure 32 – Regular vs. Failed Vacuum Tube Performance

Vacuum loss can occur due to poor manufacturing, but more likely due to a combination of thermal and mechanical stress over time on the metal to glass seal. The evacuated tubes were tested during manufacturing and were able to withstand 150 lbs. of tension along the axis of the tube. They are, however, much more susceptible to stress in the radial direction, which is the stress experienced during thermal expansion of the manifold.

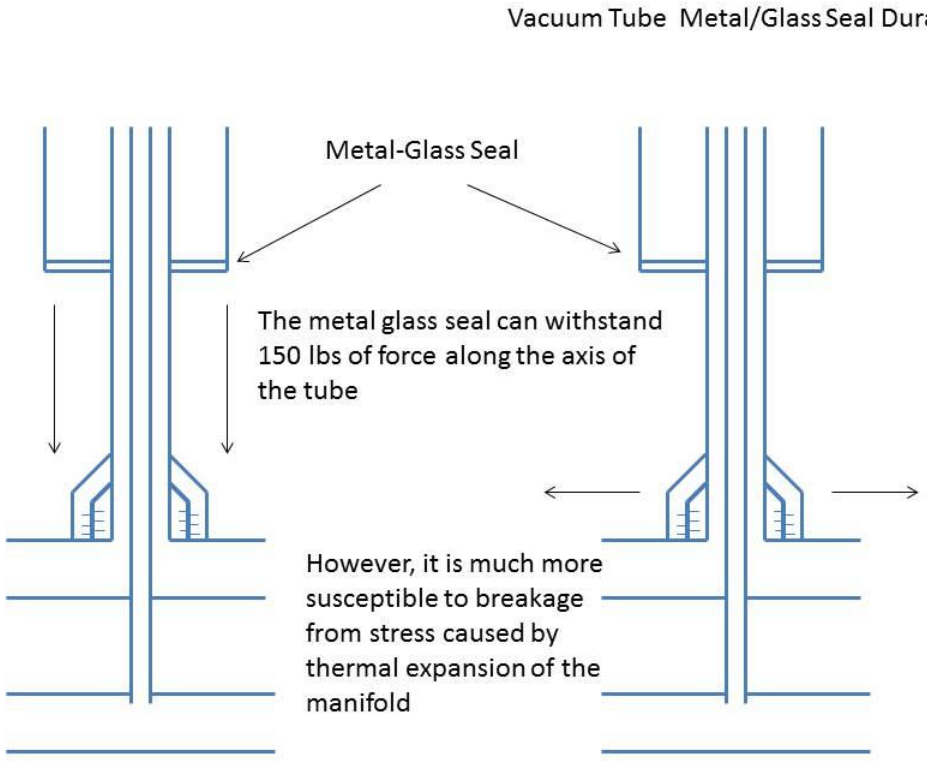

Figure 33 – Metal/Glass Seal Durability

Basically, the tubes are held in place by the plastic troughs but the manifold is allowed to expand due to the flexible hoses between manifolds. This causes a daily bending of the copper connector of the vacuum tube and a daily stress on the metal to glass seal. Currently we have not attempted to solve this problem, but a few

possible solutions exist. First, and probably the easiest, is lengthening the copper connector from the tube to the manifold might provide enough flexibility to absorb the small shifts caused by thermal expansion of the manifold. Second, the plastic troughs could be situated on a floating frame that can shift with the expanding manifolds. Finally, a new material for the manifold could be used that has a smaller coefficient of expansion. At the writing of this thesis, since we have no more vacuum tubes, we are going to run the system for another cooling season to determine the extent of vacuum loss and to determine how many more tubes we will need to purchase.

5. Conclusion and Closing Comments

In this thesis, the design and performance of a solar cooling system using a new type of concentrator is presented and analyzed. The XCPC collectors, when operated in the temperature range of 150 – 180 °C, achieved daily efficiencies of 36.7% with instantaneous efficiencies up to 40%. The double effect absorption chiller maintained a COP between 0.97 and 1.14 and the thermal COP of the system averaged at 1.0. The solar COP of the entire system was 0.363 with very little variation.

This is the first system of its kind to combine XCPC (External Compound Parabolic Concentrator) technology with double effect absorption chilling technology. The purpose of this demonstration was to prove the XCPC's competency at providing thermal power for space cooling and in this sense it was a success. The XCPC operates at efficiencies comparable to those reached by tracking type solar collectors and the power production window coincides nicely with the desired window for space cooling. At the same time, the XCPC is able to collect diffuse light, allowing for

cooling during cloudy or hazy days, which is especially important in regions with high diffuse percentage. The effects of dust settling on efficiency is briefly investigated and presented and a discussion on the importance of designing a system with a low thermal mass to decrease warm up times is presented. A discussion of parasitic losses and a simple economic analysis are also presented for completion.

The main obstacles that were faced by our solar cooling team are listed here with the hopes of providing valuable information for building a better system in the future. We have offered a number of possible solutions to these problems, but since changing one parameter (i.e. type of metal of manifold, location of manifold on collector, etc.) invariably affects a multitude of other parameters in the system, these solutions are only speculative until they are incorporated into the next system.

Ultimately, while more research needs to be done in the areas of long term and yearly performance, integration with building loads, and system level optimization, this project has successfully demonstrated the use of the XCPC in providing thermal power for space cooling applications.

Figure 34 – XCPC array at UC Merced Castle research facility

Appendix A – Matlab Code

vacuumTube.m was used to model the efficiency of a regular tube and a tube that has lost vacuum. The results from this model are shown in Figure 32.

```
%Vacuum Tube Finite Difference Model
%INCLUDES EFFECTS OF GLASS AND ABSORBER
%AS WELL AS EFFECTS OF VARYING DEGREE OF VACUUM (eta_vac)
%INPUT RADIATION IS INCIDENT ON OUTER SURFACE OF GLASS
%Bennett Widyolar - 2012

function [T_fluid_in, T_fluid_out, T_abs, T_go, qRad] =
vacuumTube(mdot, G, T_in, T_amb, Tube_flag, Coating_flag, eta_vac)
% G = INCIDENT RADIATION ON U-TUBE (OUTSIDE OF GLASS)
% mdot = MASS FLOW RATE THROUGH TUBE IN Kg/s
% T_in = INLET TEMPERATURE OF FLUID
% T_amb = AMBIENT TEMPERATURE
% Tube_flag = [1 = U-tube, 2 = Counter-flow Tube]
% Coating_flag = [1 = TiNOX, 2 = Eurocon, 3 = Mirotherm]
% eta_vac = Vaccum Parameter (0 = Full Vaccum, 1 = No Vacuum)

%PROGRAM VARIABLES
n = 50;                         %[#] Number of sub-divisions
tol = 0.0001;                   %[C] PROGRAM TOLERANCE (WHEN TO END
ITERATION)

%ABSORBER
[l_abs, D_abs] = getTubeDim();
dx = l_abs/(n-1);               %[m] Differential Length of Absorber
A_abs = pi*D_abs*l_abs;          %[m^2] Total Surface Area of Absorber
dA_abs = pi*D_abs*dx;            %[m^2] Differential Area of Absorber

%GET ABSORPTANCE OF SELECTIVE COATING
[alpha_abs,~] = getCoating(T_in,Coating_flag);

%GLASS
l_glass = 1.8;                  %[m] Length of Glass Shell
D_gi = 61.8e-3;                 %[m] Inner Diameter of Glass Shell
D_go = 65e-3;                   %[m] Outer Diameter of Glass Shell
A_gi = pi*D_gi*l_glass;          %[m^2] Inner Surface Area of Glass Shell
A_go = pi*D_go*l_glass;          %[m^2] Outer Surface Area of Glass Shell

tao_glass = 0.917;              %[%] TRANSMISIVITY OF GLASS IN VISIBLE
RANGE
emis_glass = 1;                 %[%] ABSORPTIVITY OF GLASS IN IR RANGE
k_glass = 1.005;                %[W/m-K] Thermal Conductivity of PYREX
GLASS (ENGINEERING TOOLBOX)

%RADIATION CONSTANTS
F12 = 1;                        %[%] VIEW FACTOR DIFFERENTIAL ABSORBER TO
GLASS
```

```
F21 = F12*dA_abs/A_gi;      %[%] VIEW FACTOR GLASS TO DIFFERENTIAL
ABSORBER
F22 = 1-(F21*(n-1));        %[%] VIEW FACTOR GLASS TO GLASS
F11 = 0;                    %[%] VIEW FACTOR ABSORBER TO ABSORBER

sigma = 5.67e-8;            %[W/m^2-K^4]

%BUILD VIEW FACTOR MATRIX
F(1:n-1,1:n-1) = F11;
F(1:n-1,n) = F12;
F(n,1:n-1) = F21;
F(n,n) = F22;

%HEAT TRANSFER CONSTANTS
h = 100;                %[W/m^2-K] HTC for Counter-Flow Tube-to-Fluid
h_amb = 10;             %[W/m^2-K] HTC for Glass to Ambient
k_cu = 400;             %[W/m-K] Thermal Conductivity of Copper
h_air = 100*eta_vac;    %[W/m-K] HTC for Absorber/Glass to Air inside
Tube

%INITIAL GUESSES
T_fluid_in_guess(1:n,1) = T_in;         %[C]
T_fluid_out_guess(1:n,1) = T_in;        %[C]
T_abs_guess(1:n-1,1) = T_in + 20;       %[C]
T_air_guess = 80;                       %[C]
T_gi_guess = 40;                        %[C]
T_go_guess = T_gi_guess;                %[C]

loop = 1;               %[0 = off | 1 = on] Loop Variable
count = 0;              %[#] Loop Counter

if (Tube_flag == 1)

    %U-TUBE PIPE
    D_i = 6.5e-3;               %[m] Inner Radius of Pipe
    D_o = 8e-3;                 %[m] Outer Radius of Pipe

    Ai = pi*D_i*dx;             %[m^2]
    Ao = pi*D_o*dx;             %[m^2]

    if (Coating_flag == 1)    %TiNOX HAS 2mm WELD
        A_weld = (2e-3)*dx;
        h_weld = 250000;
    else                      %ALL OTHERS ARE HALF OUTER PIPE SURFACE
        A_weld = Ao;
        h_weld = 150;
    end

    while (loop && count <= 50)
        count = count + 1;

        %FINITE DIFFERENCE MODEL SOLVED BY MATRIX INVERSION
        %[A]*[C] = [B]
```

```
        %[A] = Coefficient Matrix
        %[C] = Temperature Matrix (i.e. Temperature of all surfaces)
        %[B] = Constants Matrix
        %[C] = A\B (TEMPERATURES SOLVED BY MATRIX INVERSION)

        %INITIALIZE MATRICES
        A = zeros(7*n+3,7*n+3);
        B = zeros(7*n+3,1);

        %GET FLUID PROPERTIES
        cp_i = hcap_oil(T_fluid_in_guess)*1000;         %[J/Kg-K] Heat
Capacity
        cp_o = hcap_oil(T_fluid_out_guess)*1000;        %[J/Kg-K] Of
Fluid
        %GET EMISSIVITY OF ABSORBER IN IR RANGE
        [~,emis_abs] = getCoating(T_abs_guess,Coating_flag);

        %BUILD SIMULTANEOUS EQUATION MATRIX

        %FLUID IN - SUPPLY SIDE
        A(1,1) = 1;                      %INITIAL CONDITION
        B(1,1) = T_fluid_in_guess(1);    %INLET TEMPERATURE OF FLUID

        for i = 2:n
            A(i,i-1) = -mdot*cp_i(i) + h*Ai;
            A(i,i) = mdot*cp_i(i);
            A(i,i+n-1) = -h*Ai;             %[NOTE: i+n-1 -> SEE
STAGGERING]
            B(i,1) = 0;
        end

        %PIPE INNER SURFACE - SUPPLY SIDE
        for i = n+1:2*n-1                   %[NOTE: n-1 -> SEE
STAGGERING]
            A(i,i-n) = -h*Ai;
            A(i,i) = h*Ai + 2*pi*k_cu*dx/log(D_o/D_i);
            A(i,i+n) = -2*pi*k_cu*dx/log(D_o/D_i);
            B(i,1) = 0;
        end
        A(2*n,2*n) = 1;                 %Node is not used but must be
filled
        B(2*n,1) = 1;                   %to keep square matrix

        %PIPE OUTER SURFACE - SUPPLY SIDE
        for i = 2*n+1:3*n-1                 %[NOTE: n-1 -> SEE
STAGGERING]
            A(i,i-n) = -2*pi*k_cu*dx/log(D_o/D_i);
            A(i,i) = 2*pi*k_cu*dx/log(D_o/D_i) + h_weld*A_weld;
            A(i,i+4*n) = -h_weld*A_weld;
            B(i,1) = 0;
        end
        A(3*n,3*n) = 1;                 %Node is not used but must be
filled
        B(3*n,1) = 1;                   %to keep square matrix
```

```
        %FLUID OUT - RETURN SIDE
        %NODE [4*n] IS SAME TEMP AS OUTLET FROM SUPPLY PIPE
        A(4*n,4*n) = 1;
        A(4*n,n) = -1;
        B(4*n,1) = 0;

        for i = 3*n+1:4*n-1
            A(i,i+1) = -mdot*cp_o(i-3*n) + h*Ai;
            A(i,i) = mdot*cp_o(i-3*n);
            A(i,i+n) = -h*Ai;
            B(i,1) = 0;
        end

        %PIPE INNER SURFACE - RETURN SIDE
        for i = 4*n+1:5*n-1           %[NOTE: n-1 -> SEE STAGGERING]
            A(i,i-n+1) = -h*Ai;    %[NOTE: i-n+1 -> FLOW DIRECTION
CHANGE]
            A(i,i) = 2*pi*k_cu*dx/log(D_o/D_i) + h*Ai;
            A(i,i+n) = -2*pi*k_cu*dx/log(D_o/D_i);
            B(i,1) = 0;
        end
        A(5*n,5*n) = 1;                %Node is not used but must be
filled
        B(5*n,1) = 1;                  %to keep square matrix

        %PIPE OUTER SURFACE - RETURN SIDE
        for i = 5*n+1:6*n
            A(i,i-n) = -2*pi*k_cu*dx/log(D_o/D_i);
            A(i,i) = 2*pi*k_cu*dx/log(D_o/D_i) + h_weld*A_weld;
            A(i,i+n) = -h_weld*A_weld;
            B(i,1) = 0;
        end
        A(6*n,6*n) = 1;
        B(6*n,1) = 1;

        %BUILD AND SOLVE RADIATION MATRIX
        epsilon = emis_abs;
        epsilon(n,1) = emis_glass;
        [D,E] = buildRadiationMatrix(F,epsilon,n);
        sol = sigma*((T_abs_guess+273).^4);
        sol(n,1) = sigma*((T_gi_guess+273)^4);
        qRad = D\(E*sol);

        %ABSORBER
        rad_in_direct = tao_glass*alpha_abs*G;
        rad_in_reflect = tao_glass*(1-alpha_abs)*(1-tao_glass)*(1-
F22)*alpha_abs*G;
        for i = 6*n+1:7*n-1
            A(i,i-n) = -h_weld*A_weld;
            A(i,i-4*n) = -h_weld*A_weld;
            A(i,i) = 2*h_weld*A_weld + h_air*dA_abs;
            A(i,7*n+1) = -h_air*dA_abs;
```

```
            B(i,1) = dA_abs*(rad_in_direct + rad_in_reflect - qRad(i-
6*n));
        end
        A(7*n,7*n) = 1;                 %Node is not used but must be
filled
        B(7*n,1) = 1;                   %to keep square matrix

        %AIR INSIDE TUBE
        for i = 6*n+1:7*n-1
            A(7*n+1,i) = -h_air*dA_abs;
        end
        A(7*n+1,7*n+1) = h_air*A_gi + h_air*A_abs;
        A(7*n+1,7*n+2) = -h_air*A_gi;
        B(7*n+1,1) = 0;

        %INNER GLASS SURFACE
        A(7*n+2,7*n+1) = -h_air*A_gi;
        A(7*n+2,7*n+2) = 2*pi*k_glass*dx/log(D_go/D_gi) + h_air*A_gi;
        A(7*n+2,7*n+3) = -2*pi*k_glass*dx/log(D_go/D_gi);
        B(7*n+2,1) = -A_gi*qRad(n);

        %OUTER GLASS SURFACE
        rad_glass = emis_glass*sigma*((T_go_guess+273)^4 -
(T_amb+273)^4);
        A(7*n+3,7*n+3) = A_go*h_amb + 2*pi*k_glass*dx/log(D_go/D_gi);
        A(7*n+3,7*n+2) = -2*pi*k_glass*dx/log(D_go/D_gi);
        B(7*n+3,1) = A_go*h_amb*T_amb - A_go*rad_glass;

        %SOLVE SYSTEM OF EQUATIONS
        C = A\B;

        %OUTPUT TEMPERATURE PROFILES
        T_fluid_in = C(1:n);
        T_fluid_out = C(3*n+1:4*n);
        T_abs = C(6*n+1:7*n-1);
        T_air = C(7*n+1);
        T_gi = C(7*n+2);
        T_go = C(7*n+3);
        %CHANGE IN TEMPS PER ITERATION
        d_T_fi = abs(T_fluid_in - T_fluid_in_guess);
        d_T_fo = abs(T_fluid_out - T_fluid_out_guess);
        d_T_abs = abs(T_abs - T_abs_guess);
        d_T_air = abs(T_air - T_air_guess);
        d_T_go = abs(T_go - T_go_guess);
        d_T_gi = abs(T_gi - T_gi_guess);

        %CHECK TO SEE IF DONE
        loop = 0;
        for i = 1:n
            if (d_T_fi(i) > tol || d_T_fo(i) > tol)
                loop = 1;
            end
            if (i < n-1 && d_T_abs(i) > tol)
                loop = 1;
```

```
            end
        end
        if (d_T_go > tol || d_T_gi > tol || d_T_air > tol)
            loop = 1;
        end

        %SET GUESSES AS CALCULATED TEMPS
        T_fluid_in_guess = T_fluid_in;
        T_fluid_out_guess = T_fluid_out;
        T_abs_guess = T_abs;
        T_air_guess = T_air;
        T_gi_guess = T_gi;
        T_go_guess = T_go;
    end

end
```

References

[1] US Energy Information Administration, Annual Energy Outlook 2012, Jan. 2012 http://www.eia.doe.gov/emeu/aer/txt/ptb0201a.html.

[2] US Department of Energy, Buildings Energy Data Book, 2011 http://buildingsdatabook.eren.doe.gov/ChapterIntro1.aspx

[3] Kulkarni, P.P., 1994. Solar absorption cooling for demand-side management, Energy Engineering, **91**(5), 29-39.

[4] International Energy Agency, Solar Heating and Cooling Programme. Solar Cooling Position Paper. Task 38 Solar Air-Conditioning and Refrigeration. October 2011

[5] Summerer, F. Ziegler, F. Riesch, P. Alefeld, G. 1966. Hydroxide Absorption Heat Pumps with Spray Absorber. American Society of Heating Refrigeration and Air Conditioning Engineers, **102**, 1010-1018.

[6] Schweigler, C. J. Riesch, P. Demmel, S. Alefeld, G. 1966. A New Absorption Chiller to Establish Combined Cold, Heat, and Power Generation Utilizing Low-Temperature Heat. American Society of Heating Refrigeration and Air Conditioning Engineers, **102**, 1118-1127.

[7] Tim Berlitz, Bostjan Cerkvenik, Hans-Martin Hellmann, Felix Ziegler. 2001. The impact of work input to sorption cycles, International Journal of Refrigeration, **24**, 88-99

[8] Nunez, T. et al, 2005. Development of an adsorption chiller and heat pump for domestic heating and air-conditioning applications. Applied Thermal Engineering, **27**, pp 2205-2212.

[9] Henning, H.-M. et al, 2005. Micro tri-generation system for indoor air conditioning in the Mediterranean climate. Applied Thermal engineering, **27**, pp 2188-2194.

[10] Gommed, K, Grossman G, Ziegler F. 2004. Experimental Investigation of a LiCl-water Open Absorption System for Cooling and Dehumidification, Transactions of the ASME, **126**, 710-715

[11] Henning, H.-M. 2006. Solar assisted air conditioning of buildings – an overview. Applied Thermal Engineering, **27**, pp. 1734-1749.

[12] Jin-Soo Kim, Felix Ziegler, Huen Lee. 2002. Simulation of the compressor-assisted triple-effect H2O/LiBr absorption cooling cycles, Applied Thermal Engineering, **22**, 295-308

[13] A. Syed et al, 2005, A novel experimental investigation of a solar cooling system in Madrid, International Journal of Refrigeration, **28**, pp. 859-871.

[14] Agyenim F. et al, 2010, Design and experimental testing of the performance of an outdoor
LiBr/H2O solar thermal absorption cooling system with a cold store, Solar energy, **84**, pp. 735-744.

[15] A. Mammoli et al, 2010, Energetic, economic and environmental performance of a solar-thermal-assisted HVAC system, Energy and Buildings, **42**, pp. 1524-1535.

[16] P. Bermejo, 2010, Solar absorption cooling plant in Seiville, Solar Energy, **84**, pp. 1503-1512.

[17] M. Qu et al, 2010, A solar thermal cooling and heating system for a building: Experimental and model based performance analysis and design, Solar energy, **84**, pp. 166-182.

[18] W. Duff et al, 2004, Performance of the Sacramento demonstration ICPC collector and double effect chiller, Solar energy, **76**, pp. 175-180.

[19] Winston, R. 2012, Thermodynamically efficient solar concentrators, J. Photon Energy, **2**(1), 025501. doi:10.1117/1.JPE.2.025501

[20] Winston, R. 2009. Design and Development of Low-cost, High-temperature, Solar Collectors for Mass Production. California Energy Commission PIER Public Interest Energy Research Program Report: CEC-500-05-021

[21] Broad X Non-Electric Chiller, Model Selection and Design Manual. Broad Central Air Conditioning (Absorption LiBr + H20). Sept. 2008

[22] Poiry, Heather. Efficient Solar Cooling.

[23] Balkoski, Kevin. Performance Analysis of Medium Temperature Non-Tracking Solar Thermal Concentrators.